Available online at www.sciencedirect.com
ScienceDirect
Geochimica et Cosmochimica Acta 74 (2010) 6387–6405
Geochimica et Cosmochimica Acta
www.elsevier.com/locate/gca

# Rare Earth Element and yttrium compositions of Archean and Paleoproterozoic Fe formations revisited: New perspectives on the significance and mechanisms of deposition

Noah Planavsky [a,b,*], Andrey Bekker [c], Olivier J. Rouxel [b,d], Balz Kamber [e], Axel Hofmann [f], Andrew Knudsen [g], Timothy W. Lyons [a]

[a] Department of Earth Sciences, University of California, Riverside, Riverside, CA 92521, USA
[b] Department of Marine Chemistry and Geochemistry, Woods Hole Oceanographic Institute, Woods Hole, MA 02543, USA
[c] Department of Geological Sciences, University of Manitoba, Winnipeg, MB, Canada R3T 2N2
[d] University of Brest, European Institute for Marine Studies, Technopôle Brest-Iroise, Place Nicolas Copernic, 29280 Plouzané, France
[e] Department of Geology, Laurentian University, Sudbury, ON, Canada P3E 2C6
[f] School of Geological Sciences, University of Kwazulu-Natal, Durban 4000, South Africa
[g] Department of Geology, Lawrence University, Appleton, WI 54912, USA

Received 16 December 2009; accepted in revised form 6 July 2010; available online 25 July 2010

**Abstract**

The ocean and atmosphere were largely anoxic in the early Precambrian, resulting in an Fe cycle that was dramatically different than today's. Extremely Fe-rich sedimentary deposits—i.e., Fe formations—are the most conspicuous manifestation of this distinct Fe cycle. Rare Earth Element (REE) systematics have long been used as a tool to understand the origin of Fe formations and the corresponding chemistry of the ancient ocean. However, many earlier REE studies of Fe formations have drawn ambiguous conclusions, partially due to analytical limitations and sampling from severely altered units. Here, we present new chemical analyses of Fe formation samples from 18 units, ranging in age from ca. 3.0 to 1.8 billion years old (Ga), which allow a reevaluation of the depositional mechanisms and significance of Precambrian Fe formations. There are several temporal trends in our REE and Y dataset that reflect shifts in marine redox conditions. In general, Archean Fe formations do not display significant shale-normalized negative Ce anomalies, and only Fe formations younger than 1.9 Ga display prominent positive Ce anomalies. Low Y/Ho ratios and high shale-normalized light to heavy REE (LREE/HREE) ratios are also present in ca. 1.9 Ga and younger Fe formations but are essentially absent in their Archean counterparts. These marked differences in Paleoproterozoic versus Archean REE + Y patterns can be explained in terms of varying REE cycling in the water column.

Similar to modern redox-stratified basins, the REE + Y patterns in late Paleoproterozoic Fe formations record evidence of a shuttle of metal and Ce oxides across the redoxcline from oxic shallow seawater to deeper anoxic waters. Oxide dissolution—mainly of Mn oxides—in an anoxic water column lowers the dissolved Y/Ho ratio, raises the light to heavy REE ratio, and increases the concentration of Ce relative to the neighboring REE (La and Pr). Fe oxides precipitating at or near the chemocline will capture these REE anomalies and thus evidence for this oxide shuttle. In contrast, Archean Fe formations do not display REE + Y patterns indicative of an oxide shuttle, which implies an absence of a distinct Mn redoxcline prior to the rise of atmospheric oxygen in the early Paleoproterozoic. As further evidence for reducing conditions in shallow-water environments of the Archean ocean, REE data for carbonates deposited on shallow-water Archean carbonate platforms that stratigraphically underlie Fe formations also lack negative Ce anomalies. These results question classical models for deposition of Archean Fe formations that invoke oxidation by free oxygen at or above a redoxcline. In contrast, we add to growing

* Corresponding author. Address: Department of Earth Sciences, University of California, Riverside, Riverside, CA 92521, USA. Tel.: +1 951 452 6227.
*E-mail address:* planavsky@gmail.com (N. Planavsky).

0016-7037/$ - see front matter © 2010 Elsevier Ltd. All rights reserved.
doi:10.1016/j.gca.2010.07.021

evidence that metabolic Fe oxidation is a more likely oxidative mechanism for these Fe formations, implying that the Fe distribution in Archean oceans could have been controlled by microbial Fe uptake rather than the oxidative potential of shallow-marine environments.
© 2010 Elsevier Ltd. All rights reserved.

## 1. INTRODUCTION

Fe formations are extensively studied, but still poorly understood, sedimentary rocks composed predominantly of authigenic iron-bearing carbonates, silicates, and oxides in a siliceous matrix. These marine chemical precipitates are often characterized by alternating Fe-rich and Fe-poor layers and therefore are commonly referred to as banded Fe formations (BIFs; Holland, 2005; Klein, 2005). Fe formations host the majority of the world's economic Fe ore, which has fostered extensive research on their origin, depositional setting, and spatial and temporal distribution. There have been several recent reviews on Fe formations (Klein, 2005; Ohmoto et al., 2006; Beukes and Gutzmer, 2008; Bekker et al., 2010).

The basic conditions leading to deposition of Fe formations in ancient oceans are generally agreed upon (Holland, 2005). Fe formations appear to be deposited either in close association with volcanic activity (Algoma-type Fe formations) or on submerged platforms on continental shelves more distal to submarine volcanic activity (Superior-type Fe formations) (Klein, 2005; Beukes and Gutzmer, 2008). The precursor particles to both types of Fe formations precipitated from seawater containing micromolar levels of dissolved ferrous Fe (Holland, 1973). A substantial marine ferrous Fe reservoir was possible due to: (1) a reducing atmosphere or one with a low oxidizing potential (Holland, 1984; Bekker et al., 2004); (2) low marine sulfate and sulfide concentrations (Canfield and Teske, 1996; Habicht et al., 2002); and (3) a high hydrothermal Fe flux (Kump and Seyfried, 2005). These conditions persisted, at least episodically, until the late Paleoproterozoic around 1.8 Ga (Holland, 1984; Poulton et al., 2004; Slack et al., 2007). Deposition of Fe formations appears to have been pulsed; the most significant periods occurred during emplacement of large igneous provinces, which enhanced hydrothermal Fe discharge (Barley et al., 1997; Isley and Abbott, 1999).

In contrast, detailed mechanisms involved in the deposition of Fe formations remain poorly resolved despite more than a century of investigation (Klein, 2005; Ohmoto et al., 2006; Beukes and Gutzmer, 2008). The classical and most widely accepted model for Fe formation deposition invokes ambient free oxygen induced ferrous Fe oxygenation. This model, championed by Preston Cloud (e.g., Cloud, 1965), suggests that deposition of Fe formation occurred at the interface between oxygenated shallow waters and upwelling Fe-rich reduced waters. The oxidizing shallow waters have been linked to prolific communities of oxygenic photosynthesizers (Cloud, 1965, 1973).

Metabolic ferrous Fe oxidation was also proposed as a mechanism for Fe formation deposition. The potential importance of microaerophilic microbial Fe oxidation has been recognized for almost a century (Harder, 1919). Anoxygenic photosynthetic oxidation, photoferrotrophy, is another metabolic Fe oxidation pathway linked to Fe formation deposition by Garrels and Perry (1974) almost 20 years before organisms capable of this type of metabolism were cultured (Widdel et al., 1993). More recently, organisms able to metabolically couple Fe oxidation to nitrate reduction have been discovered (e.g., Edwards et al., 2003), providing another possible microbially mediated mechanism for deposition of Fe formations.

It was also proposed that Fe formations may be purely abiogenic products. Many Fe formations are composed predominantly of Fe carbonates or Fe silicates suggested to be abiotic marine precipitates (e.g., Sumner, 1997; Ohmoto et al., 2004). However, siderite in most Fe formations shows highly negative carbon isotope values, consistent with dissimilatory Fe reduction and formation of siderite during early diagenesis (Walker, 1984; Kaufman et al., 1990; Fischer et al., 2009). Fe isotopes also appear to provide a signature for diagenetic siderite formation (Johnson et al., 2004, 2008).

UV-induced ferrous Fe oxidation has also been advanced as an important mechanism (Braterman et al., 1983; Anbar and Holland, 1992), but the efficiency of UV-dependent oxidation in complex seawater solutions has been questioned (e.g., Konhauser et al., 2007). Ferrous Fe oxidation in hydrothermal fluids due to phase separation is yet another possible mechanism for Algoma-type Fe formation deposition (Foustoukos and Bekker, 2008), but this process cannot explain Superior-type Fe formations deposited on stable continental shelves away from submarine volcanic activity.

We have conducted a geochemical study on bulk samples from 18 different Fe formations ranging in age from the Archean to the Paleoproterozoic, bracketing the rise of atmospheric oxygen at ca. 2.4 Ga (Bekker et al., 2004), with the goal of better defining the mechanisms behind Fe formation deposition through time. Our study focuses on Rare Earth Element (REE) and yttrium (Y) concentrations in Fe formations, but we also present data for microbialite-dominated marine carbonates deposited on a shallow-water Archean carbonate platform. Both Fe formations and microbially mediated carbonates, as chemical precipitates, are well suited to trace element studies. These lithologies appear to be robust proxies for seawater composition, as long as contamination by clastic sediment and late-stage metamorphism/alteration are well understood (e.g., Bau and Dulski, 1996; Webb and Kamber, 2000; Kamber and Webb, 2001; Slack et al., 2007). By examining both shallow (carbonate) and deepwater (Fe formation) depositional environments it is possible to get a complete view of the ocean redox structure. An understanding of water-column redox structure is necessary to distinguish among competing models for the origin of Fe formations. Since Y is

geochemically similar to the heavy REE Ho but displays different complexion properties in marine systems (Ho is scavenged on particulate matter two times faster than Y; Nozaki et al., 1997), we also use Y/REE ratios to elucidate paleoceanographic processes.

Although REEs have long been used to elucidate mechanisms of Fe formation genesis, the conclusions of many previous studies are compromised by inaccurate or incomplete REE analyses and by a limited number of measurements, as discussed by Bau and Dulski (1996). Earlier studies focused mainly on Ce and Eu anomalies as proxies for ocean redox state and hydrothermal flux, respectively. Our study differs from previous work by focusing on evidence for an oxide shuttle from shallow oxic to deeper anoxic waters in late Paleoproterozoic oceans and in highlighting that this process appears to have been absent in the Archean and early Paleoproterozoic.

## 2. MATERIALS AND METHODS

### 2.1. Sample description

We are using a definition for Fe formation that differs slightly from that of Klein (2005). For our purposes, siliceous and Fe-rich sedimentary chemical precipitates with low levels of detrital siliciclastic or volcaniclastic material (<1% $Al_2O_3$) and greater than 10% total Fe are considered to be Fe formations, regardless of whether Fe is associated with a carbonate or oxide phase. This composition-based definition of Fe formation encompasses both granular and banded Fe formations as well as ferruginous cherts (e.g., distal hydrothermal jaspers). For comparison, we also present data for ferruginous shales associated with Fe formations to demonstrate the effect of siliciclastic material on REE patterns. Basic sample information, mineralogy, as well as major and trace element compositions are presented in Appendix Tables 1A, 1B and 2.

We also investigated the Mosher carbonates of the ca. 2.9 Ga Steep Rock Group from the Superior Province. The Mosher carbonates offer insight into shallow-water marine conditions; these carbonates are composed of seafloor precipitates that span a significant bathymetric gradient (Kusky and Hudleston, 1999; Fralick et al., 2008). Past work has confirmed that authigenic carbonate precipitates are well suited to reconstructing basin-scale changes in seawater composition (e.g., REEs, Fe, Mn; see Kamber and Webb, 2001; Sumner and Grotzinger, 2004).

### 2.2. Methods

Clean rocks were crushed between two plexiglass discs inside a Teflon bag using a hydraulic press. Rock chips were rinsed several times with deionized water during ultrasonication. The cleaned material was powdered in an agate shatterbox. In some cases, we removed material from the crushed chips containing significant detrital component (e.g., lenses of siliciclastic sediments) using a binocular microscope.

Sample powders were weighed in 5 mL Teflon beakers and dissolved using 2 mL of concentrated trace metal grade $HNO_3$ with 2 mL of concentrated HF. After evaporation on a hot plate at 50 °C, complete dissolution and Fe oxidation were achieved by a second evaporation step using 4 mL of *aqua regia*. The dry residue was then dissolved in 4 mL of 6 N HCl and one drop of $H_2O_2$ by heating at 40 °C in a closed vessel. Organic carbon was not attacked by this procedure and was always present in trace amounts. Carbonates were dissolved in pre-cleaned 14 mL polypropylene test tubes in 5% sub-boiling triple-distilled $HNO_3$.

Analyses of REEs + Y and Ba were performed on a ThermoElectron Inc. Element2 inductively coupled plasma–mass spectrometer (ICP–MS) at the Woods Hole Oceanographic Institution (WHOI) and on a ThermoElectron Inc. XSeriesII ICP–MS at Laurentian University. At WHOI, solutions were injected into the plasma using a Cetac Aridus® desolvating nebulizer to reduce isobaric interferences (e.g., $^{135}Ba^{16}O^+$ on $^{151}Eu^+$). Formation of Ba and REE oxides was monitored throughout the analytical session by periodic aspiration of Ba and Ce spikes. Ba–oxide formation was significantly less than 1% of the total Ba in solution. Any isobaric interference of $BaO^+$ on $Eu^+$ would have decreased the measured $^{151}Eu/^{153}Eu$ ratio below that naturally occurring (~0.89). In almost all samples no bias was observed, and no correction for BaO interference was required. REE–oxide formation was typically less than ~4% of total REE concentration. Samples were spiked with 5 ppb of internal In standard to correct for fluctuations of the plasma during the analytical session. Unknown sample concentrations were calibrated against matrix-matched, multi-REE standards prepared with Specpure plasma solution standards. Background intensities were measured periodically by aspirating 5% $HNO_3$ blanks. Accuracy of our analyses is conservatively estimated to be ±10%, and Rare Earth Element ratios are estimated to be accurate within ±5%, based on multiple analyses of randomly selected samples across multiple analytical sessions. Analytical precision and the accuracy of our measurements of REE abundances and ratios were also checked by multiple analyses of the geostandards IF-G and BHVO-1 (Table 2). Reproducibility at WHOI was better than 5% for all REEs + Y.

We analyzed trace element concentrations at Laurentian University using a method modified from Eggins et al. (1997), which employs internal standards ($^6$Li, In, Re, Bi, and $^{235}U$) and external drift correction. The instrument was tuned to 1.5% $CeO^+/Ce^+$, and all isobaric interferences were corrected using oxide formation rates determined for pure elemental solution measured immediately after sample analysis. With this method, REE in basaltic rock standards such as BHVO-1 and -2 can be reproduced to better than 1% rsd using a quartz spray chamber (see Kamber, 2009, for more information). Carbonates normally have low trace element concentrations, and precision for carbonate samples was consequently only better than 2% for all REEs + Y.

Major elements in the Fe formation samples (Fe, Al, Ca, and Mg) were determined using the medium-resolution mode of the *Element II* at WHOI with a quartz spray chamber. Similarly to the REE procedure, In was used as an internal standard, and the data were calibrated by standardization to the geostandard BHVO-1. Analytical precision and accuracy of element abundances were checked by multiple analyses of the geostandards IF-G and

BHVO-2; reproducibility was better than 5%. Selected samples representative of the various matrices were sent to Activation Laboratories Ltd. (Ancaster, Ontario) for additional geochemical analysis. Major and trace elements were analyzed at Activation Laboratories by ICP-AES and ICP-MS, respectively, after lithium metaborate/tetraborate fusion. Major element compositions and REE anomalies determined by both techniques are reproducible within 5%.

## 3. RESULTS

### 3.1. Rare Earth Elements in Fe formations

We observe several temporal trends in REE patterns normalized to shale composites (Post-Archean Australian Shale—PAAS), hereafter referred to as $REE_{(SN)}$ (Fig. 1). First, none of the samples of Fe formation contain statistically significant negative $Ce_{(SN)}$ anomalies. True negative $Ce_{(SN)}$ anomalies, as defined in Fig. 2, have Ce/Ce* ($Ce_{(SN)}/(0.5Pr_{(SN)} + 0.5La_{(SN)})$) and Pr/Pr* ($Pr_{(SN)}/(0.5Ce_{(SN)} + 0.5Nd_{(SN)})$) values less than and greater than unity, respectively. This approach, described by Bau and Dulski (1996), discriminates between positive La and true negative $Ce_{(SN)}$ anomalies. Positive $Ce_{(SN)}$ anomalies are not present in our samples older than ca. 1.9 Ga (Fig. 2).

Second, late Paleoproterozoic Fe formations display a much wider range of light-to-heavy REE ratios compared to the older Fe formations. Light-to-heavy REE ratios are calculated as the $Pr_{(SN)}/Yb_{(SN)}$ ratio (Fig. 1C). Early Paleoproterozoic and Archean Fe formations are characterized by light REE depletion, while the late Paleoproterozoic examples show a wide range of light-to-heavy REE ratios that are well above and below the ratio of the shale composite (Fig. 1C). Fe formations with a significant siliciclastic contribution are characterized by shale-like, flat REE patterns.

Thirdly, there are significant differences in the shale-normalized behavior of Y in late Paleoproterozoic Fe formations compared to those of early Paleoproterozoic and Archean age. The Archean and early Paleoproterozoic examples have positive $Y_{(SN)}$ anomalies (Fig. 1D). The average Y/Ho ratio for Archean and early Paleoproterozoic Fe formations in our sample set is 39, which is markedly higher than the shale composite ratio of ~27. In contrast,

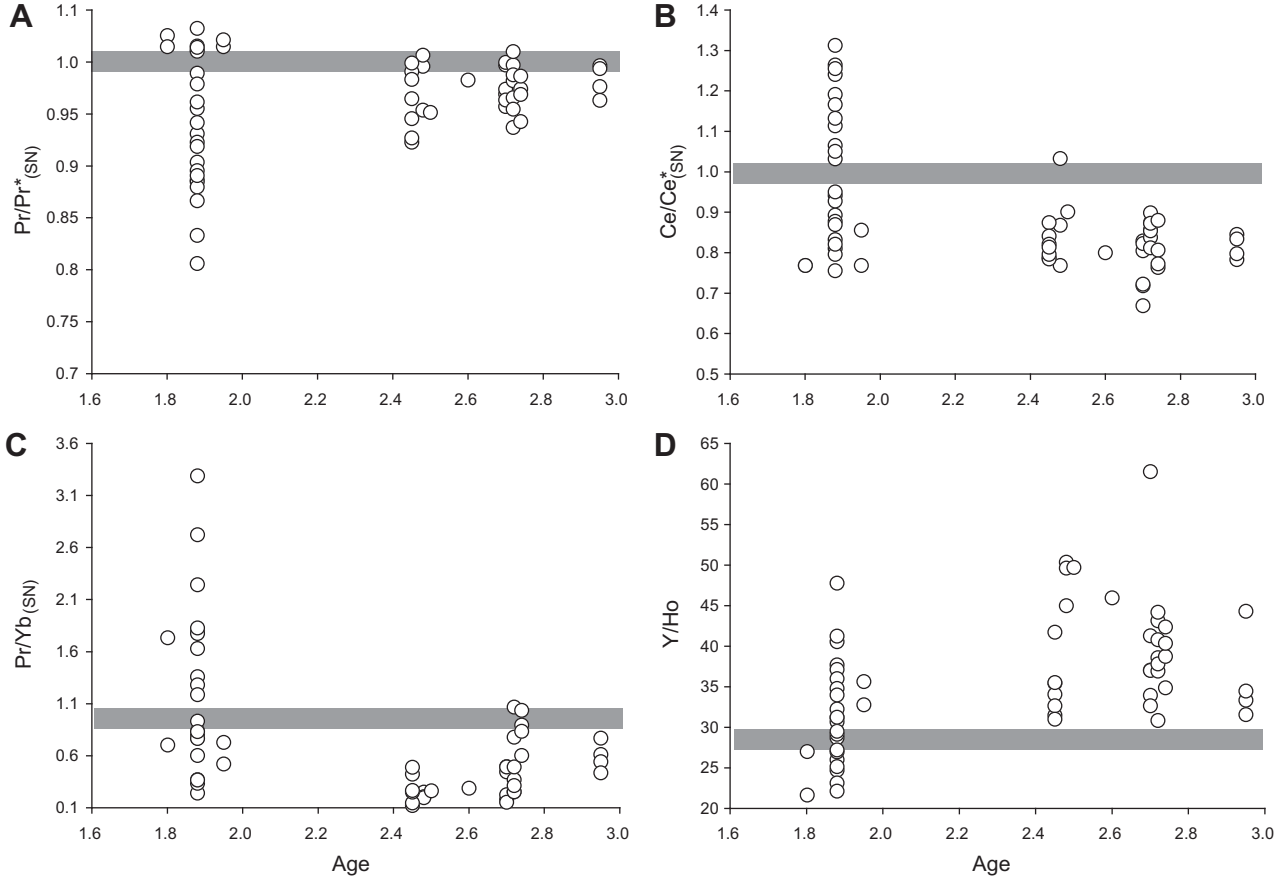


Fig. 1. Temporal trends in REE + Y characteristics of Fe formations. (A) Pr anomalies ($Pr_{SN}/(0.5(Ce_{SN} + Nd_{SN})$. (B) Ce anomalies ($Ce_{SN}/(0.5(Pr_{SN} + La_{SN})$. (C) Light to heavy REE ratios ($Pr/Yb_{SN}$). (D) Y/Ho ratios. Black bar indicates PAAS shale composite values. Positive $Ce_{SN}$ anomalies are not present in Archean Fe formations but are common in late Paleoproterozoic Fe formations. Archean Fe formations are characterized by higher Y/Ho ratios than that of shale composite and lower light to heavy REE ratios than that of shale composite, while late Paleoproterozoic Fe formation have a large range of Y/Ho and light to heavy REE ratios. The observed temporal trend in REE + Y characteristics is best explained by the absence of a Fe–Mn redoxcline in the Archean oceans prior to the rise of atmospheric oxygen (see text for details).

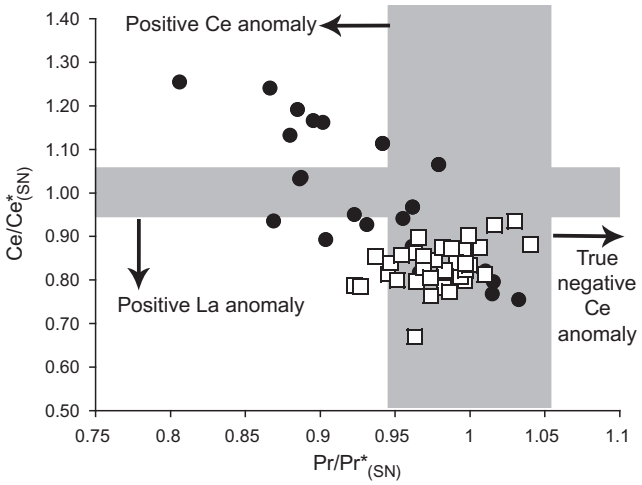


Fig. 2. Plot of $Ce_{SN}$ and $Pr_{SN}$ anomalies for late Paleoproterozoic (●) and Archean and early Paleoproterozoic (□) Fe formations. Positive Ce anomalies are only present in late Paleoproterozoic Fe formations whereas all analyzed Fe formations do not display true negative Ce anomalies. True negative Ce anomalies are defined by $Ce/Ce^*_{SN}$ ($Ce_{SN}/(0.5(Pr_{SN} + La_{SN})$ and $Pr/Pr^*_{SN}$ ($Pr_{SN}/(0.5Ce_{SN} + 0.5Nd_{SN})$) values above and below the unity, respectively. The approach first described by Bau and Dulski (1996) discriminates between positive La and true negative Ce anomalies.

late Paleoproterozoic Fe formations have a wide range of Y/Ho ratios, both above and below the shale composite value, with an average Y/Ho ratio for our sample set of 32. Ferruginous shales—that is, samples with more than 5% $Al_2O_3$—are characterized by Y/Ho ratios that are similar to that of the shale composite.

Finally, nearly all of the analyzed Fe formations contain significant positive shale-normalized Eu anomalies. Eu anomalies are calculated as $Eu_{(SN)}/(0.66Sm_{(SN)} + 0.33\ Tb_{(SN)})$ because seawater can have a slight positive Gd anomaly. $Eu_{(SN)}$ anomalies range from 1.01 to 4.29 and have an average of 2.1 for Archean and late Paleoproterozoic Fe formations. The late Paleoproterozoic examples contain lower $Eu_{(SN)}$ anomalies, ranging from 1.15 to 2.46 with an average of 1.5.

### 3.2. Rare Earth Elements in Mosher carbonates

Carbonates sampled from the Steep Rock Group have REE + Y concentrations that vary from 0.01 to 6.26 ppm. These REE concentrations are similar to those reported for other non-skeletal carbonates with only low concentrations of the elements associated with clastic sediment, such as Ga and Zr. Concentrations of Zr in the Mosher carbonates vary from 0.02 to 0.27 ppm, which is much less than the shale composite values of ~200 ppm. The Mosher carbonates have shale-normalized REE patterns similar to those of the Archean and early Paleoproterozoic Fe formations (Fig. 3). Specifically, the patterns lack significant negative $Ce_{(SN)}$ anomalies (Fig. 4), are light $REE_{(SN)}$-depleted, have Y/Ho ratios higher than shale composites, and exhibit positive $Eu_{(SN)}$ anomalies. On a Ce and Pr anomaly scatter diagram (Fig. 4), the Steep Rock carbonates plot in the same field as Archean Fe formations and ca. 2.5 Ga Campbellrand carbonates. It is interesting to compare the Mosher and Campbellrand carbonates since they both were deposited in shallow-water environments and stratigraphically underlie Fe formations. Their $Ce_{(SN)}$ and $Pr_{(SN)}$ anomalies are distinct from those observed in modern (e.g., Webb and Kamber, 2000) and early Phanerozoic (e.g., Nothdurft et al., 2004) non-skeletal and microbial carbonates (Fig. 4). The Steep Rock $Eu_{(SN)}$ anomalies ($Eu_{(SN)}/(0.66Sm_{(SN)} + 0.33Tb_{(SN)})$) range from 2.75 to 3.86, which is, on average, higher than the values seen in the analyzed Archean Fe formations or in the Campbellrand carbonates.

There are similar correlations (Fig. 5) between REE characteristics in the Mosher carbonates and those in the Campbellrand carbonates (Kamber and Webb, 2001), likely linked with water-column REE fractionations. Similar to the Campbellrand carbonates, within the Mosher carbonates there is a correlation between $Ce_{(SN)}$ and $Y_{(SN)}$ anomalies and between both $Ce_{(SN)}$ and $Y_{(SN)}$ anomalies and the degree of light REE depletion (Fig. 5). Variation in the $Ce_{(SN)}$ anomaly of the Mosher carbonates reflects La-enrichment rather than non-conservative Ce behavior, given the limited range of the $Pr_{(SN)}$ anomalies (Fig. 4; cf. Kamber and Webb, 2001). There is not a strong correlation between the $Eu_{(SN)}$ anomalies and either Y/Ho or $Pr_{(SN)}/Yb_{(SN)}$ ratios either the Campbellrand or Steep Rock carbonates (Fig. 5D).

## 4. DISCUSSION

### 4.1. REE signatures of redox-stratified basins and their preservation in marine Fe-oxide deposits and carbonates

REE behavior in modern redox-stratified basins is well known. The capture and preservation of aqueous REE patterns in marine chemical precipitates provides a window into ancient ocean chemistry and redox state. In general, oxygenated modern marine settings display a strong negative $Ce_{(SN)}$ anomaly when normalized to shale composites, while suboxic and anoxic waters lack significant negative $Ce_{(SN)}$ anomalies (German and Elderfield, 1990; Byrne and

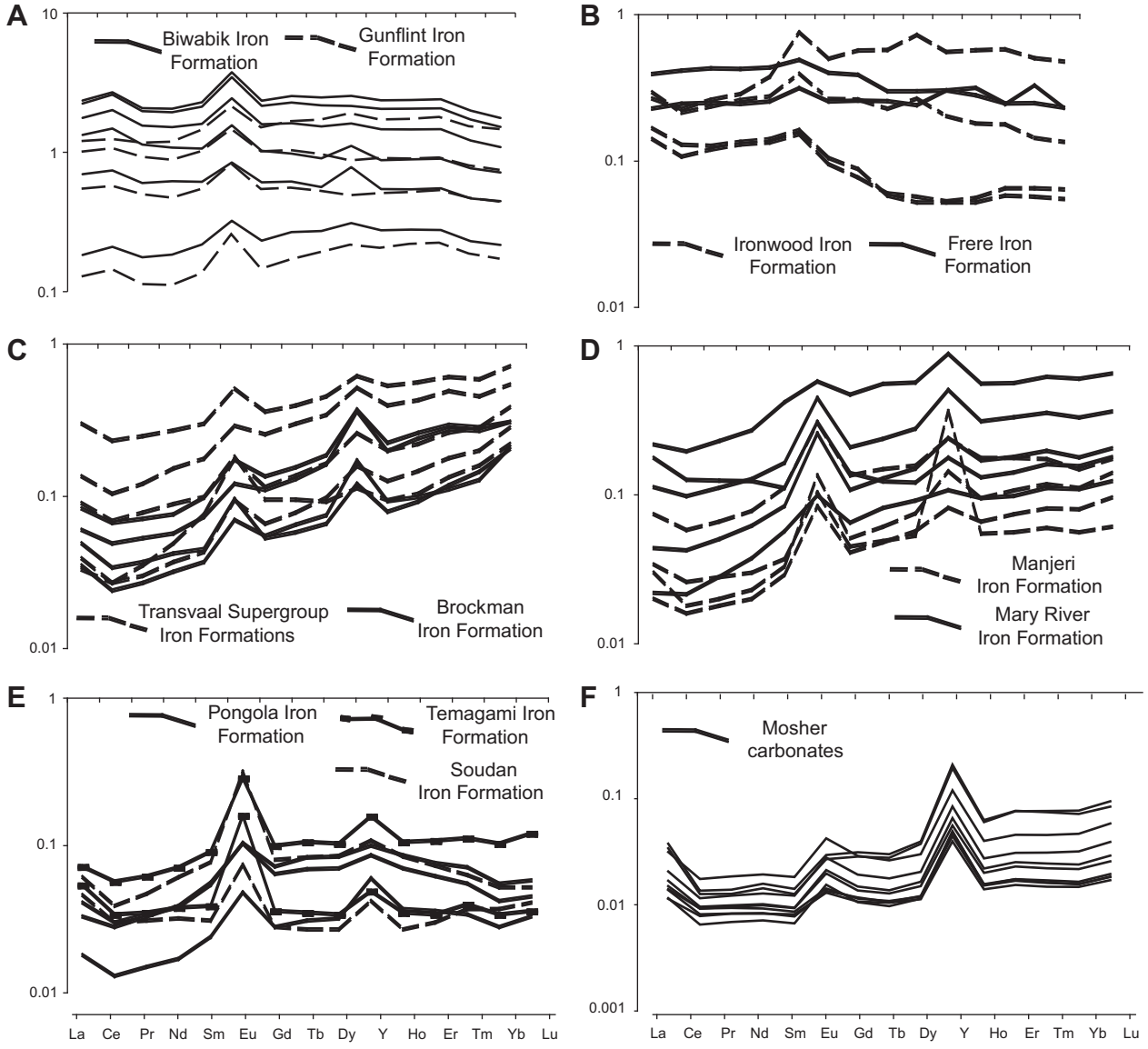


Fig. 3. Shale-normalized (PAAS) REE patterns for representative samples of late Paleoproterozoic (A and B), early Paleoproterozoic (C), and Archean (D and E) Fe formations and carbonates from the Steep Rock Group (F).

Sholkovitz, 1996). Essentially following German and Elderfield (1990), we consider waters suboxic if they contain low levels of dissolved oxygen (0.05–5 μmol $O_2$) and no dissolved sulfide. Oxidation of Ce(III) greatly reduces Ce solubility, resulting in preferential removal onto Mn–Fe oxyhydroxides, organic matter, and clay particles (Byrne and Sholkovitz, 1996). In contrast, suboxic and anoxic waters lack significant negative $Ce_{(SN)}$ anomalies due to reductive dissolution of settling Mn–Fe-rich particles (German et al., 1991; Byrne and Sholkovitz, 1996). Similarly, light REE depletion develops in oxygenated water bodies due to preferential removal of light versus heavy REEs onto Mn–Fe oxyhydroxides and other reactive surfaces due to differential REE particle reactivity, which is linked with REE carbonate complexation. The ratio of light to heavy REEs increases markedly across redox boundaries due to reductive dissolution of Mn–Fe oxyhydroxides (Sholkovitz and Elderfield, 1988; German et al., 1991; Sholkovitz et al., 1992; Byrne and Sholkovitz, 1996, see also Fig. 6A). In many redox-stratified basins the $Ce_{(SN)}$ anomaly and the light to heavy REE ratio return to near-shale composite values across the Mn and Fe redox boundaries. In some basins, however, positive $Ce_{(SN)}$ anomalies and light REE enrichment develop in anoxic and suboxic waters due to reductive dissolution (de Baar et al., 1988; Schijf et al., 1995; Bau et al., 1997b; De Carlo and Green, 2002). Redox-induced change in REE patterns in some modern redox-stratified basins can be linked directly to Mn cycling in the suboxic zone (German et al., 1991; De Carlo and Green, 2002).

Yttrium displays the inverse behavior of light REEs and Ce in redox-stratified basins. It is less particle-reactive than its geochemical analog Ho, resulting in Y/Ho ratios in marine environments that are higher than shale composites (Bau

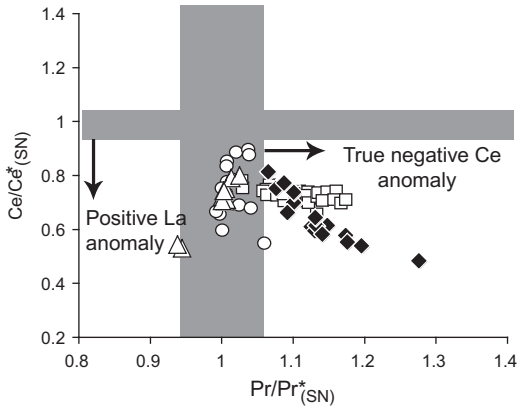


Fig. 4. Plot of $Ce_{SN}$ and $Pr_{SN}$ anomalies in microbialite-containing carbonates of the ca. 2.8 Ga Steep Rock Group (△) and ca. 2.52 Ga Campbellrand Subgroup (Kamber and Webb, 2001; ○). Carbonates of the Devonian Canning Basin (Nothdurft et al., 2004; ♦) and Holocene Herron Island (Webb and Kamber, 2000; □) are also shown for comparison. The Archean carbonates lack true negative Ce anomalies in contrast to Devonian and Holocene carbonates. The Steep Rock and Campbellrand carbonates suggest that the shallow-water high-productivity Archean carbonate platforms had a low oxidizing potential.

et al., 1997b; Nozaki et al., 1997). Since the difference in Y and Ho particle reactivity is well expressed in metal oxides, there is a decrease in dissolved seawater Y/Ho ratios in suboxic and anoxic waters driven by an increase in Ho relative to Y as Mn–Fe-rich particles dissolve (Bau et al., 1997b).

Marine sediments rich in authigenic Fe and non-skeletal carbonates have been shown to provide a qualitative record of seawater REE and Y patterns (e.g., Bau and Dulski, 1996; Bau, 1999; Kamber and Webb, 2001; Nothdurft et al., 2004; Bau and Alexander, 2006; Slack et al., 2007). Fe oxides at close to neutral pH record Ce anomalies and REE patterns of the water column from which they precipitated qualitatively, in contrast to Mn oxides that scavenge Ce and heavy REE preferentially (Bau, 1999; De Carlo et al., 2000; Ohta and Kawabe, 2001). For instance, particles from Mn-poor hydrothermal plumes essentially record a seawater REE pattern (e.g., Sherrel et al., 1999). There is preferential Ho relative to Y sorption onto Fe oxides at circum-neutral pH (Bau, 1999), but particles from modern Mn-poor hydrothermal plumes nevertheless record near-seawater Y/Ho ratios that are notably higher than ratios of shale composites (e.g., Edmonds and German, 2004).

The primary, near-seawater REE patterns in carbonate precipitates and Fe oxide-rich sediments are unlikely to

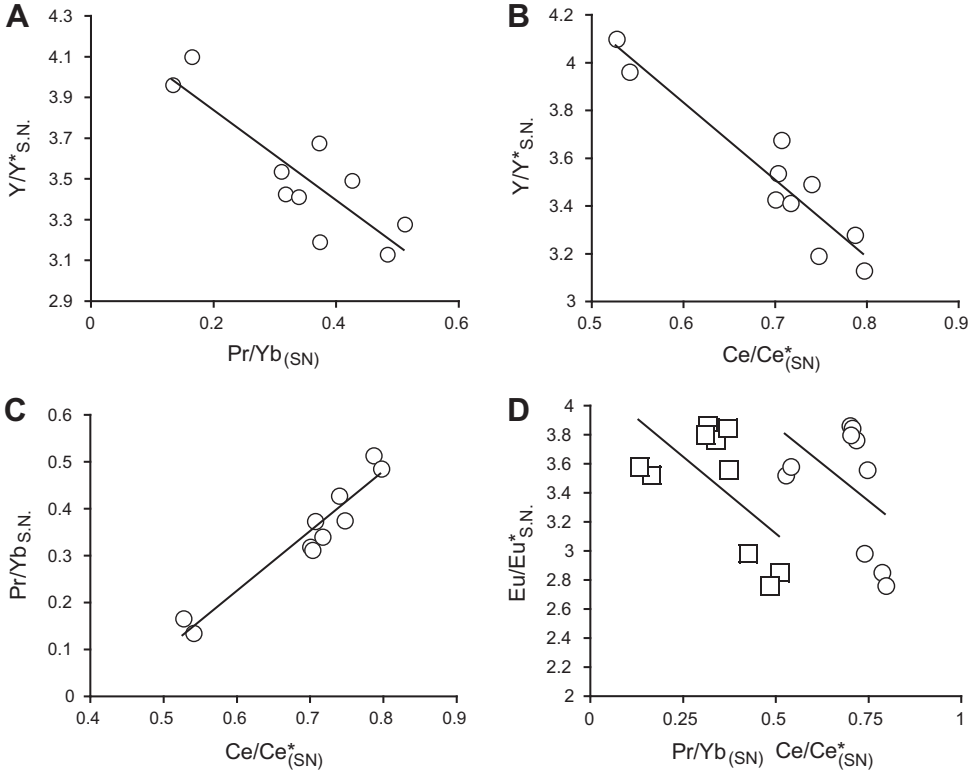


Fig. 5. Cross-plots of REE + Y characteristics of the Mosher carbonates from the Steep Rock Group. (A) Y anomalies ($Y_{SN}/(Er_{SN} + Ho_{SN})$ versus the light to heavy REE ratios ($Pr_{SN}/Yb_{SN}$). (B) Y anomalies versus Ce anomalies ($Ce_{SN}/(0.5(Pr_{SN} + La_{SN})$. (C) Light to heavy REE ratios ($Pr_{SN}/Yb_{SN}$) versus Ce anomalies. Co-variation between Y anomalies, Ce anomalies, and light to heavy REE ratios is consistent with oceanographic REE + Y processing. The Ce anomalies likely reflect non-conservative La behavior given the lack of significant Pr anomalies. The lack of significant Ce anomalies despite evidence for oceanographic REE + Y processing indicates that the water column on the shallow water, high-productivity Steep Rock carbonate platform was reducing with respect to Ce and Mn. (D) Eu anomalies ($Eu_{SN}/(0.66 * Sm_{SN} + 0.33 * Tb_{SN})$ versus Ce anomalies (○) and light to heavy REE ratios ($Pr_{SN}/Yb_{SN}$) (□). Weak negative correlation between Eu anomalies and apparent Ce anomalies, reflecting La anomalies, and Eu anomalies and light to heavy REE ratios suggests mixing between deep hydrothermally dominated seawater and shallow waters affected by REE scavenging on particles and organic matter.

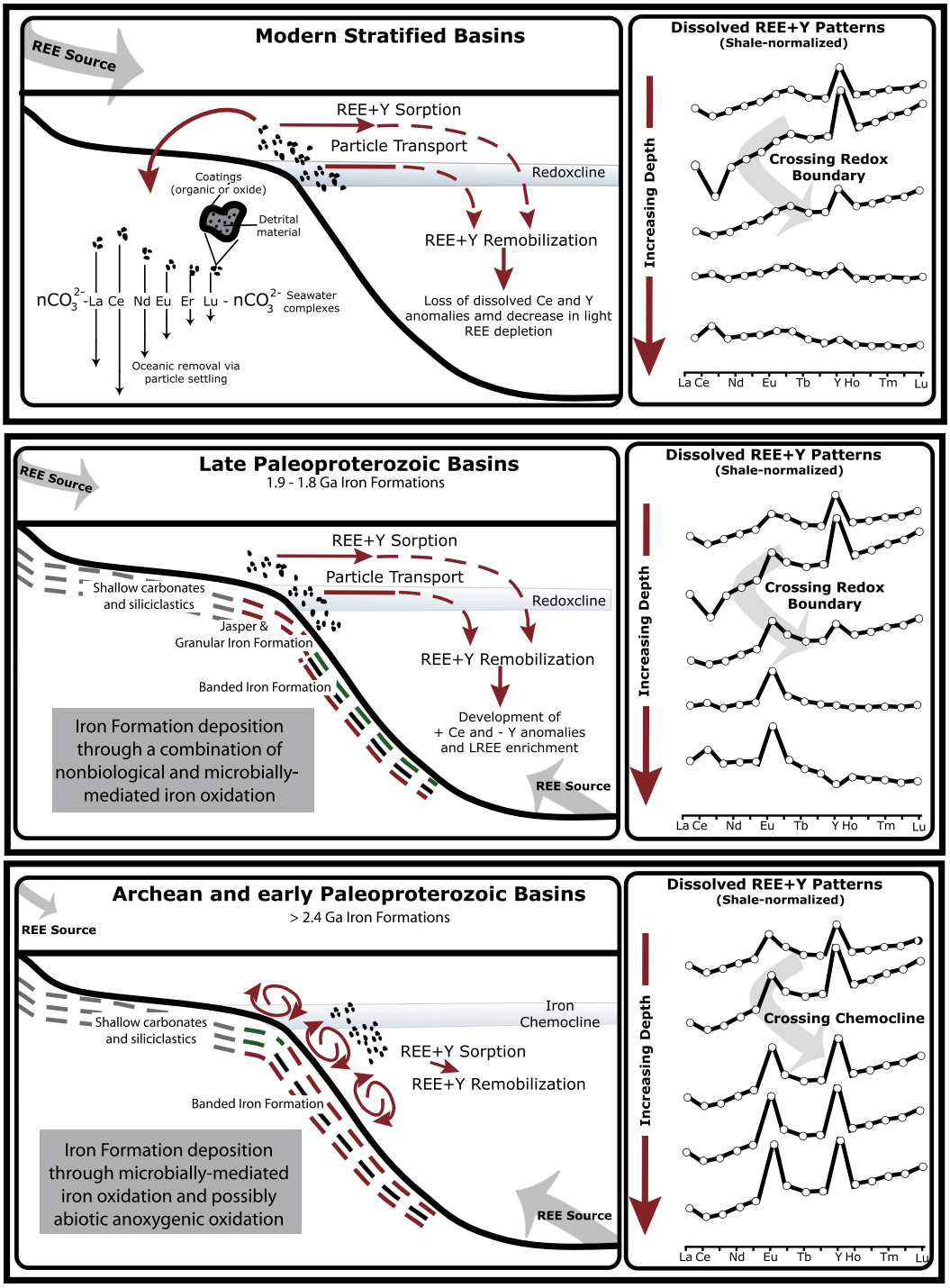


Fig. 6. Model for the evolution of ocean redox structure based on new REE analyses of 18 Fe formations with ages ranging from ca. 3.0 Ga to 1.88 Ga. Fe formations can serve as a qualitative proxy for seawater REE pattern and, therefore, offer insight into the evolution of marine redox conditions. Similarly to modern redox-stratified basins (A), the REE + Y pattern of late Paleoproterozoic Fe formations (B) records evidence for a shuttle of metal and Ce oxides from oxic shallow seawater across the redoxcline. Oxide, mainly Mn oxide, dissolution in anoxic water column lowers the Y/Ho ratios, raises the light to heavy REE ratios, and increases the Ce concentration relative to neighboring REE (La and Pr). In contrast, Archean Fe formations do not display REE + Y pattern indicative of an oxide shuttle (C), which implies a lack of significant Mn cycling across redoxcline prior to the rise of atmospheric oxygen in the early Paleoproterozoic. The model for REE particle sorption shown in (A) is redrafted from Sholkovitz et al. (1994).

change significantly during typical burial diagenesis and metamorphism. REEs in siliceous, Fe oxide-rich sediments and non-skeletal carbonates appear to be rock buffered under the low water–rock ratios typical of most early to late-

stage diagenetic and metamorphic conditions (Bau, 1993). REE sorption to Fe oxides and dissolved speciation are strongly influenced by aquatic carbonate chemistry (e.g., Moller and Bau, 1993; Quinn et al., 2006). However, the marine carbonic acid system is likely to have been constant enough through Earth's history (e.g., Holland, 1984) that this characteristic does not undermine the paleoproxy potential of REE. One significant caveat is that carbonate and siliceous Fe oxide-rich sediments can be useful as a paleoceanographic proxy only if their siliciclastic contents are very low (Kamber and Webb, 2001; Nothdurft et al., 2004). Thus, Fe oxides and non-skeletal carbonates essentially record the REE patterns of the waters from which they precipitated. These patters are likely to be retained as the sediments become rock and experience low grade metamorphism (e.g., Bau and Dulski, 1996; Slack et al., 2007).

### 4.2. Rare Earth Element patterns in Fe formations as tracers of ancient ocean redox

The observed temporal trends in REE patterns in Fe formations likely reflect the long-term evolution of marine redox structure. The absence of any deviations from trivalent Ce behavior in Archean and early Paleoproterozoic Fe formations in our dataset suggests that the basins in which Fe formations were deposited were reducing with respect to Ce. Cerium has a redox potential close to Mn, indicating that the water column remained reducing with respect to Mn prior to the rise in atmospheric oxygen at ca. 2.4 Ga (Bekker et al., 2004). In contrast, ca. 1.9 Ga Fe formations deposited after the rise of atmospheric oxygen commonly show positive Ce anomalies. The positive Ce anomalies indicate an oxidative Ce cycle in combination with a shuttle of Mn oxyhydroxide particles across a redoxcline. Dissolution of these metal oxyhydroxides would have increased the seawater dissolved Ce content. As seen in some modern basins (de Baar et al., 1988; Bau et al., 1997b; De Carlo and Green, 2002), this dissolution would at times have led to the formation of positive dissolved Ce anomalies in deeper, anoxic–suboxic waters. Positive Ce anomalies would be transferred to the sedimentary record when Fe oxyhydroxide precipitation occurred in these suboxic or anoxic waters. Positive Ce anomalies in samples of ca. 1.9 Ga Mn-poor Fe formation likely indicate a dissolved positive Ce anomaly, given that experimental work suggests (in contrast to Mn oxides) that minimal or no preferential Ce scavenging onto Fe oxyhydroxides occurs in the pH range relevant to marine conditions (Koeppenkastrop and De Carlo, 1992; Bau, 1999).

We propose that the observed temporal trend in trivalent REE + Y patterns also reflects evolution of marine redox structure. Light REE depletion and high Y/Ho ratios in Archean and early Paleoproterozoic Fe formations are at odds with the assumption that Fe oxide precipitation occurred in the transition zone between oxic and anoxic waters. Under such transitional conditions, as described above for modern redox-stratified basins, significant variability is expected in light-to-heavy REE and Y/Ho ratios, with variability induced by oxidative scavenging and reductive dissolution. By analogy to these modern settings, we would also expect nearly flat aqueous REE patterns and low Y/Ho ratios in the water column near the Mn redoxcline (Fig. 6). These patterns should be recorded in Fe oxide-rich sediments if the ferrous Fe oxidation and ferric Fe particle formation (the precursor particles of to Fe formations) occurred in low oxygen conditions. We see evidence for this oxide shuttle in late Paleoproterozoic Fe formations, which have significant ranges in both Y/Ho and light-to-heavy REE ($Pr/Yb_{(SN)}$) ratios (both below and above the shale composite values). We interpret this range of light-to-heavy REE and Y/Ho ratios in late Paleoproterozoic Fe formations as a proxy for deposition in water masses with varying contributions of REE + Y from precipitation and dissolution of Mn–Fe oxyhydroxides. This interpretation implies deposition of late Paleoproterozoic Fe formations under varying redox conditions in basins with a strong redoxcline separating the oxic upper portion of the water column from the suboxic to anoxic deeper portion (Planavsky et al., 2009). In contrast, strong light REE depletion and Y enrichments in almost all Archean Fe formations suggest the absence of an oxide shuttle across a Mn redoxcline.

The wide range of Y/Ho and $Pr/Yb_{(SN)}$ ratios in late Paleoproterozoic Fe formations is unlikely to be related to basin isolation or varying degrees of detrital contribution. In the Biwabik Fe Formation of the ca. 1.9 Ga Lake Superior region (Tables 1A and 1B and 2), there is no systematic stratigraphic trend in either $Pr/Yb_{(SN)}$ or Y/Ho ratios within the LWD-99-2 drill core (Fig. 7), which penetrates the entire formation. Gradual basin isolation, potentially related to large-scale tectonic processes is, therefore, an unlikely cause for the observed range in the $Pr/Yb_{(SN)}$ and Y/Ho ratios. There is no covariation between $Pr/Yb_{(SN)}$ and Y/Ho ratios and the level of siliciclastic contribution (e.g., $Al_2O_3$; Fig. 8) in any of the examined Fe formations. Lack of significant covariation between light-to-heavy REE and Y/Ho ratios and proxies for detrital mineral contribution precludes the possibility that siliciclastic input was the predominant control over the trivalent REE + Y patterns. Similarly, there is no covariation in cross-plots of Mn concentration and REE anomalies.

### 4.3. Rare Earth Element patterns in Archean carbonates as tracers of ocean redox

The REE + Y patterns of the Archean Mosher and Campbellrand carbonates provide additional support for widespread reducing conditions during Fe formation deposition prior to the rise of atmospheric oxygen. The lack of any significant deviation from trivalent Ce behavior in these units (Fig. 4) indicates that Ce(III) oxidation was not prevalent during the Archean Eon even on shallow-water carbonate platforms. Given that Ce oxidation is kinetically inhibited, and as such is typically microbially mediated (Moffett, 1994), this conclusion does not necessarily demand that the shallow ocean was completely devoid of $O_2$. However, the lack of Ce anomalies suggests that free $O_2$ was not consistently present even at low ($<5$ μM) levels, conservatively assuming that Ce and Mn oxidation require

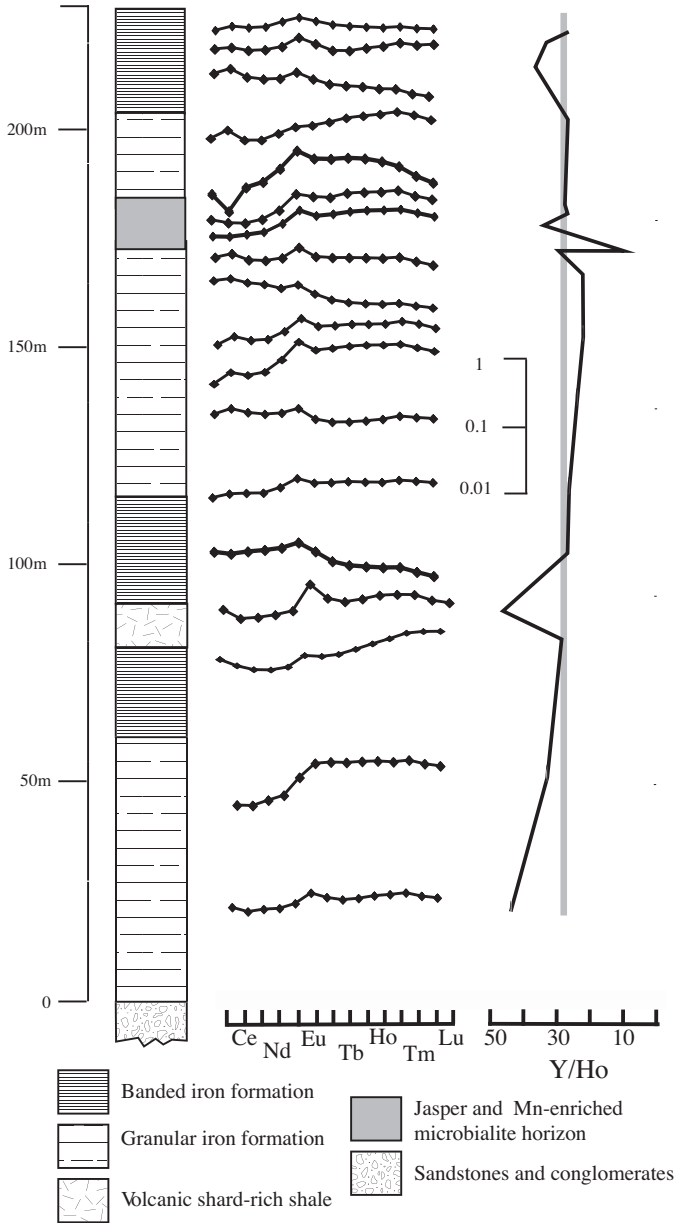


Fig. 7. REE + Y patterns for samples from the LWD-99-2 drill core through the Biwabik Fe Formation. There are large variations in the light/heavy REE and Y/Ho ratios without any systematic stratigraphic trend. Vertical dark-gray bar represents shale composite Y/Ho ratio of ~27. REE patterns (on the left) are normalized to the shale composite PAAS.

similar levels of free $O_2$ (for a case study on Mn oxidation kinetics see Clement et al., 2009).

The Mosher carbonates analyzed for REE + Y composition span a significant depth gradient. For instance, we have analyzed deeper-water fenestrate microbialites and shallow-water bioherms surrounded by grainstones (Appendix Table 3). Lack of true negative Ce anomalies is, therefore, not an artifact of local Ce maxima in surface waters (cf. Moffett, 1994). Additionally, covariation among $Pr/Yb_{(SN)}$ and Y/Ho ratios and $La_{(SN)}$ anomalies in both the Steep Rock and Campbellrand carbonates suggests aquatic REE processing, likely along a water-column depth gradient (cf. Kamber and Webb, 2001). Since Ce appears to be released preferentially during early diagenesis under reducing conditions (Byrne and Sholkovitz, 1996; Haley et al., 2004), lack of true negative $Ce_{(SN)}$ anomalies in Late Archean carbonates is unlikely to be linked to early diagenetic alteration.

Presence of strong positive $Eu_{(SN)}$ anomalies in both the Steep Rock and Campbellrand carbonates is also consistent with widespread reducing conditions. Eu enrichment in chemical sedimentary rocks precipitated from seawater indicates a strong influence of high-temperature reducing hydrothermal fluids on the dissolved REE load of seawater (cf. Klinkhammer et al., 1983; Derry and Jacobsen, 1988; Derry and Jacobsen, 1990). Presence of a hydrothermal REE signature reveals information about the redox state of the deep ocean. Under oxic conditions, hydrothermal

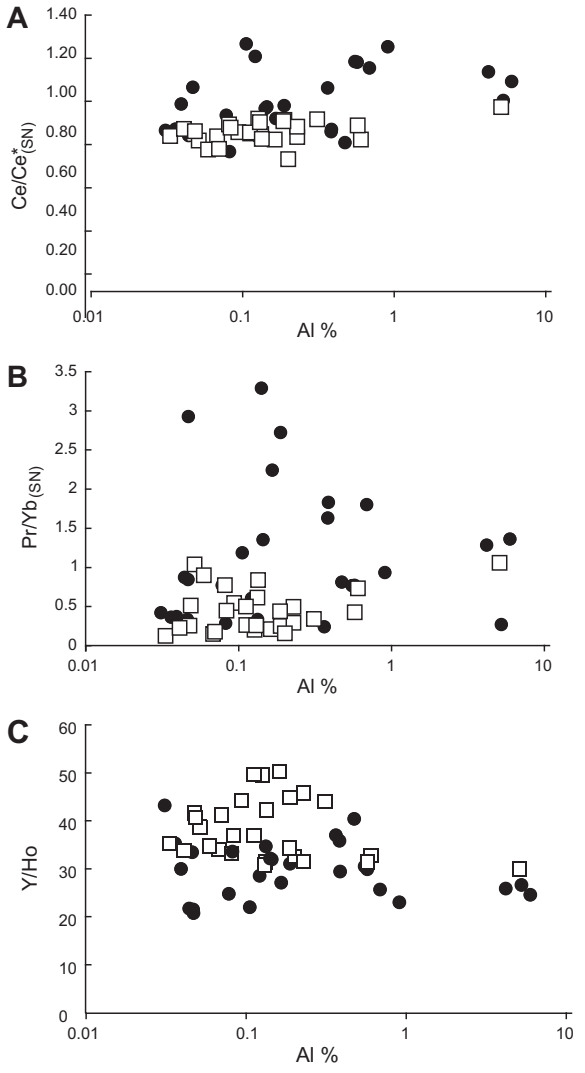


Fig. 8. Cross-plots of REE + Y characteristics and Al (wt%) for Archean and Paleoproterozoic Fe formations. (A) Ce anomalies ($Ce_{SN}/(0.5(Pr_{SN} + La_{SN})$ versus Al (wt%). (B) Light to heavy REE ratios ($Pr/Yb_{SN}$) versus Al (wt%). (C) Y/Ho ratios versus Al (wt%). Variability in the REE + Y characteristics does not correspond with degrees of detrital sediment contribution.

plumes act as a sink for seawater REEs due to their co-precipitation with Fe oxides (Kamber and Webb, 2001). Under anoxic conditions, hydrothermal systems are a REE source to the ocean.

Sedimentary features and trace element composition of Earth's earliest carbonates are also consistent with generally reducing Archean and early Paleoproterozoic shallow seawater. A predominance of *in situ* carbonate production is thought to reflect high levels of carbonate supersaturation and significant concentrations of aqueous Mn and Fe (Sumner and Grotzinger, 2004). Fe and, to a lesser extent, Mn are strong inhibitors of calcite and aragonite nucleation. Nucleation inhibition due to presence of high dissolved Fe concentrations thus provides a simple explanation for enigmatic carbonate precipitates, such as the giant aragonite fans and thick herringbone calcite beds that are common on the Steep Rock and Campbellrand carbonate platforms (Sumner, 1997; Kusky and Hudleston, 1999; Sumner and Grotzinger, 2004). Consistent with this model, well-preserved Archean limestones have Fe and Mn concentrations significantly higher than those of Proterozoic and Phanerozoic carbonates (e.g., Veizer et al., 1989). These enrichments are thought to reflect high aqueous concentrations of these metals (Sumner and Grotzinger, 2004; Veizer et al., 1989), implying reducing conditions on shallow Archean carbonate platforms.

### 4.4. Comparison with previous REE studies of Fe formations

REE studies of Fe formations have a long history (Fryer, 1976; Klein and Beukes, 1989; Derry and Jacobsen, 1990; Bau and Moller, 1993; Bau and Dulski, 1996; Kato et al., 2006; Alexander et al., 2008; Frei et al., 2008; Døssing et al., 2009), which invites a comparison between previous results and those obtained in this study. While many studies of the trace element composition of Fe formations have yielded REE + Y patterns generally consistent with the temporal trends elucidated in this study (e.g., Fryer, 1976; Bau and Moller, 1993; Bau and Dulski, 1996; Prakash and Devapriyan, 1996; Bau et al., 1997a; Alexander et al., 2008; Frei et al., 2008; Døssing et al., 2009), many others have suggested that there is a deviation from trivalent Ce behavior in Archean and early Paleoproterozoic seawater (e.g., Klein and Beukes, 1989; Kato et al., 1996, 1998, 2002, 2006; Khan and Naqvi, 1996; Ohmoto et al., 2006; Spier et al., 2007). This assertion stands in contrast to the conclusions of this study (Fig. 2). Although the significance of each reported case of negative or positive Ce anomalies in Archean rocks needs to be discussed individually, it is important to note some of the potential reasons underlying the disparity between this and previous studies of REE in Fe formations.

Many previous REE studies may be compromised by inaccurate and incomplete measurements (as reviewed in Bau and Dulski, 1996). For example, many of the REE studies that infer an oxidative Ce cycle were performed using instrumental neutron activation analysis (e.g., Klein and Beukes, 1989) rather than with more accurate and precise inductively coupled plasma mass spectrometry. Isotope dilution studies could not measure monoisotopic Pr (the neighboring element of Ce in the REE series), making it impossible to quantify Ce anomalies meaningfully. Because La displays non-conservative behavior in marine systems, the true Ce anomaly must thus be calculated using Nd and Pr (see Bau and Dulski, 1996, for discussion). ICP-MS datasets can also be affected by analytical issues. One potentially problematic issue arises when Ce, the most abundant REE in calibration standards, is analyzed in an analog detector mode, while the REE-poor BIFs and carbonates are analyzed in a pulse count mode.

Differences in sampling strategy can also account for disparities in perceived Ce behavior. For example, some of the Ce anomalies in Archean Fe formations were observed in microdrilled samples (e.g., Ohmoto et al., 2006). Our analyses, in contrast, were performed on bulk samples. Interestingly, most of the previously observed negative Ce

anomalies were documented in solitary samples, and none of these studies showed consistent Ce anomalies in stratigraphic context in a suite of representative samples. Therefore, at least some of these negative Ce anomalies likely reflect metamorphic or more recent weathering-related redistribution of REEs between metamorphic minerals and compositionally different layers or between soil horizon and bedrock. Analyzing bulk samples discriminates against these finer patterns. Although a microsampling strategy may capture interesting primary redox dynamics, this approach is more susceptible to record the effects of post-depositional redistribution. Bulk sampling should instead reveal the overall ambient primary conditions independent of local repartitioning.

Our observation of high Y/Ho ratios and light REE depletion in Archean Fe formations is generally consistent with previous work, but there are exceptions. For example, flat or light REE enriched (shale normalized) REE patterns are common in some Archean Fe formations (e.g., Kato et al., 2006). These patterns could be linked with an oxide shuttling processes as outlined above for late Paleoproterozoic Fe formations, but they could also reflect a strong hydrothermal influence, high detrital contribution, or later-stage alteration. Interestingly, similar to our findings, Frei et al. (2008), in an extensive study of Fe formations from the Black Hills area of the central United States, found that low Y/Ho ratios were much more common in Fe formations deposited after 2.4 Ga.

### 4.5. Implications of Rare Earth Element patterns for the origin of Fe formations

Our REE study provides evidence for redox evolution in the Archean to late Paleoproterozoic ocean, which has mechanistic implications for the production of Fe formation. Late Paleoproterozoic examples display a clear REE signature of ocean redox stratification and Fe formation deposition under varying redox conditions. Thus, the late Paleoproterozoic Fe formations appear to have formed through a combination of abiotic Fe oxidation at a redox interface and Fe oxidation under suboxic or anoxic conditions, which was likely microbially mediated. Archean and early Paleoproterozoic Fe formations, in contrast, do not show REE patterns indicative of deposition from a water column with a Fe–Mn redoxcline. Archean and early Paleoproterozoic carbonate successions deposited under conditions shallower than those of the basinal metalliferous sediments also contain REE patterns indicative of persistently reducing conditions. Thus, the late Paleoproterozoic and older Fe formations hold signatures of differing ocean redox structure, which suggests different modes of formation. Given the lack of evidence for either a Mn oxide shuttle or marked redox stratification as well as the apparently low oxidizing potential of shallow-water environments in Archean and early Paleoproterozoic oceans, classical models for Fe formation genesis that assumed oxidation at or above a well-established redoxcline should be reevaluated. Constraints on ocean redox structure provided by this study, coupled with evidence for an initial Fe oxyhydroxide phase in the majority of Fe formations (Ahn and Buseck, 1990; Kaufman et al., 1990; Klein, 2005; Beukes and Gutzmer, 2008; Pecoits et al., 2009), suggest that anoxic Fe oxidation was a common process in the Archean and early Paleoproterozoic before the rise of atmospheric oxygen.

Abiotic anoxic ferrous Fe oxidation mechanisms do not currently appear to have important in Fe formation genesis in the Archean and early Paleoproterozoic. UV-driven photochemical Fe oxidation in anoxic oceans would be consistent with our geochemical results. UV photolysis, however, has not been demonstrated to be efficient in complex seawater solutions (Konhauser et al., 2007). Under otherwise anoxic conditions, hydrothermal hypersaline brines may develop oxidizing and alkaline conditions along with metal enrichments due to phase separation (into vapor and brine) and the strong affinity of transition metals for chloro-complexes. It is possible that Fe oxyhydroxides could form in these brines (Foustoukos and Bekker, 2008). However, this process cannot explain Superior-type Fe formations deposited on stable continental shelves not in the immediate proximity of submarine volcanic activity. Further, currently there is no empirical evidence that this process can occur.

In this light, the rain of ferric oxides that drove Fe formation accumulation in the Archean and early Paleoproterozoic is most likely linked with metabolic microbial Fe oxidation. Our study does not offer insights into the relative importance of photoferrotrophy, microaerophilic Fe oxidation, and nitrate-dependant Fe oxidation. The relative importance of these pathways of metabolic Fe oxidation likely varied widely among different basins and under different oceanographic conditions, but nitrate was likely insignificant in the Archean and early Paleoproterozoic anoxic oceans before the rise of atmospheric oxygen. Considering these redox constraints over metabolic pathways, photoferrotrophy (and possibly microaerophilic Fe oxidation) is the most viable biological pathway for Fe oxidation in the early Earth's anoxic oceans.

There is also a strong theoretical basis for suggesting that metabolic Fe oxidation could drive Fe formation deposition. Konhauser et al. (2002) demonstrated that even modest populations of photosynthetic Fe oxidizers could account for deposition of Fe formations, despite their inferred rapid rates of accumulation (Barley et al., 1997; Pickard, 2002, 2003). Recent modeling indicates that metabolic Fe oxidation can result in near quantitative drawdown of upwelling ferrous Fe under a wide range of ocean mixing and circulation rates (Kappler et al., 2005). Even under the present oxygenated surface conditions, photoferrotrophy is an important means of Fe oxidation in Lake Matano, a ferruginous modern redox-stratified lake in Indonesia that appears to be a good analog for the Archean ocean (Crowe et al., 2008). Our study provides empirical support for Fe formation deposition by metabolic Fe oxidation in the Archean and early Paleoproterozoic, which complements the growing mass of geobiological and microbiological evidence for the importance of this process.

Evidence for extensive metabolic Fe oxidation implies that the Fe distribution in the Archean and early Paleoproterozoic oceans could have been controlled by microbial Fe utilization rather than by the redox potential of shallow

environments. Additionally, Fe oxidizing microbial ecosystems would have used upwelling dissolved phosphorous and ammonium as well as dissolved Fe. This relationship could have forced oligotrophic conditions in many shallow environments (depending on the balance of Fe and nutrient availability), limiting the levels of oxygenic photosynthesis and allowing for persistence of reducing conditions in shallow environments. Indeed, photoferrotrophs in modern Lake Matano force oligotrophic conditions in surface waters (Crowe et al., 2008) due to microbial nutrient consumption and adsorption of dissolved phosphorous onto microbial Fe oxyhydroxides, providing a modern example of the effects of metabolic microbial Fe oxidation on ecosystem stratification and redox structure. This positive feedback favoring anoxic conditions in shallow-water environments would likely be lessened during periods of low hydrothermal Fe flux.

## 5. CONCLUSIONS

We have analyzed the REE + Y compositions of bulk samples from 18 separate Fe formations and provide a reevaluation of Fe formation trace element compositions. There are several temporal trends in our Fe formation dataset that appear to reflect the evolution of the ocean redox structure. None of the analyzed Archean and Paleoproterozoic Fe formations contains statistically significant negative shale-normalized Ce anomalies. Positive Ce anomalies are not present in our dataset until ca. 1.9 Ga. Lower Y/Ho and higher light-to-heavy REE ratios compared to those of shale composites also first appear in ca. 1.9 Ga BIFs.

The lack of significant ocean redox stratification prior to the rise of atmospheric oxygen at ca. 2.3 Ga is the most parsimonious explanation of these trends. In a stratified ocean, metal and Ce oxides from oxic waters will be transported and redissolved below the redoxcline. Mn and Ce oxide dissolution in an anoxic water column would lower the Y/Ho ratio, raise the light-to-heavy REE ratio, and increase the concentration of Ce relative to neighboring REEs. Fe oxides precipitated near the chemocline will capture these seawater REE patterns, and their settling will lead to deposition of Mn-poor Fe formations. These Fe formations will record evidence of an active oxidative Mn cycle. Evidence for this oxide shuttling appears to be absent until sometime after the early Paleoproterozoic. We also present REE data from a shallow-water Archean carbonate platform. Carbonates from this environment similarly lack Ce anomalies, providing additional evidence for the absence of a Mn redoxcline in Archean and early Paleoproterozoic oceans. However, our results do not imply a total absence of oxygen in the Earth's early oceans; transient or very low levels of free oxygen in the surface ocean are consistent with our model.

REE evidence provided in this study for evolution of Precambrian ocean redox structure also has implications for our understanding of the origin of Fe formations. Late Paleoproterozoic Fe formations display a clear REE signature indicative of basin- and potentially even ocean-scale redox stratification and deposition of Fe formation under varying redox conditions. Therefore, the late Paleoproterozoic (ca. 1.9 Ga) Fe formations appear to have formed through a combination of metabolic microbial Fe oxidation in suboxic and anoxic conditions and non-biological oxidation of Fe at a redox interface. In contrast, the lack of evidence for marked redox stratification and an oxide shuttle, along with the low oxidizing potential of shallow-water environments in Archean and early Paleoproterozoic ocean, questions the plausibility of classical models for BIF deposition, which invoke non-biological Fe oxidation at the redoxcline by free oxygen (cf. Cloud, 1973). In most cases Archean Fe formations do record a flux of ferric oxyhydroxides to the sediments, which suggests that anoxic Fe oxidation was likely a common process in Archean and early Paleoproterozoic oceans. Given the uncertainty about the importance of Fe oxidation by UV photochemistry or other anoxic Fe oxidation mechanisms in the ancient ocean (e.g., Konhauser et al., 2007), our study provides empirical evidence for metabolic Fe oxidation driving Fe formation deposition. Growing evidence for metabolic Fe oxidation in Archean and early Paleoproterozoic oceans implies that the distribution of Fe in the early ocean could have been controlled by microbial Fe utilization rather than by the oxidative potential of shallow-water environments. Episodic Fe delivery to the oceans during peaks in submarine volcanic activity could, therefore, have had dramatic impacts on ocean productivity and ecosystem structure—given that anoxygenic photosynthetic Fe oxidizers were likely important components of the early Earth's biosphere.

## ACKNOWLEDGMENTS

N.P. would like to thank Cleveland Cliffs Mining, Cliffs-Erie, and the Minnesota Department of Natural Resources for access to mines and core samples. N.P. acknowledges funding from WHOI Summer Student Fellowship Program, NSF Graduate Research Fellowship, and Lawrence University Excellence in Science Fund; A.B. from the NSF Grant EAR-05-45484, NASA Astrobiology Institute award No. NNA04CC09A, NSERC Discovery Grant, and TGI-3 program operated by the Geological Survey of Canada; and O.R. from the OCE-0647948, OCE-0550066 and Frank and Lisa Hoch Endowed Fund. T.L. acknowledges funding from the NASA Exobiology Program. We thank the following individuals for their help in the field, for access to drill cores for sampling, for providing information and their own samples for this study, and stimulating discussions: Bryan Krapež, Sharad Master, Jack Redden, Martin Often, Gene LaBerge, Garth Jackson, Mark Severson, Rick Ruhanen, and Phil Fralick. The manuscript benefited from insightful comments from K. Konhauser, R. Frei, R. Bryne, and an anonymous reviewer.

## APPENDIX A. DESCRIPTIONS OF SAMPLED FORMATIONS

### A.1. 1.88 Ga Vulcan, Negaunee, Ironwood, Gunflint, and Biwabik iron formations, Animikie Basin, USA and Canada and ca. 2.0 Ga Glen Township Formation, MN, USA

The Paleoproterozoic Animikie Basin is located in the Lake Superior region of Canada and the USA and contains several geographically separate but nearly coeval thick, iron formation-bearing sedimentary successions (Ojakangas et al., 2001). The basin extends northeastward from the Mesabi Range in north-central Minnesota (containing the

Biwabik Iron Formation) to the Gunflint Range in Ontario (containing the Gunflint Iron Formation). The Gogebic, Marquette, and Menominee ranges in north-central Wisconsin and the Upper Peninsula of Michigan lie along the eastern extension of the basin and contain the Ironwood, Negaunee, and Vulcan iron formations. The ca. 2.0 Ga Glen Township Formation is located along the western margin of the basin but represents a period of iron formation deposition preceding the Biwabik and Gunflint Iron Formations. The tectonic model for the Animikie Basin has been debated for many years. The basin has been interpreted as a foreland basin that formed in response to crustal loading during the Penokean orogeny. More recently, however, an analysis based on syntectonic intrusions and sedimentology has revitalized the notion that the iron formations formed in extensional basins north of the subduction zone during the earliest stages in the Penokean orogeny (Fralick et al., 2002; Schulz and Cannon, 2007). The Gunflint Iron Formation contains the shallowest facies in the basin and is dominated by granular iron formation. All of the iron formations, however, also contain deeper-water, finely laminated units. There are large massive sulfide deposits within the Animikie Basin but the iron formations are not directly related to them and are distal to volcanic activity, although interlayered iron formations with mafic and felsic volcanic rocks and volcaniclastic layers were documented (Fralick et al., 2002; Schneider et al., 2002). The Animikie Basin iron formations contain a wide range of lithologies, but samples included in this study are Fe carbonate- or Fe oxide-dominated. The age of Animikie Basin sedimentary units is well-constrained by several U–Pb ages on individual zircons (Fralick et al., 2002; Schneider et al., 2002).

### A.2. 1.8 Ga Frere Iron Formation, Western Australia

The Frere Iron Formation is exposed both along the southern and northern margins of the Earaheedy Basin in Western Australia and is folded into a broad east-trending, south-verging asymmetric synclinal structure, with a steep to overturned northern limb. The Frere Iron Formation was deposited in a foreland basin during a transpressional stage in the Earaheedy Basin (Krapež and Martin, 1999). The Frere Iron Formation contains both granular and well-laminated lithologies, but samples included in this compilation are from laminated facies. On the southern margin, the Frere Formation is unmetamorphosed, undeformed or only mildly deformed, forming layers that are shallow-dipping to the north. The total thickness of the formation is estimated to be about 600 m. Age constraints for the Frere Iron Formation come from detrital zircon and late-stage mineralization ages bracketing the age of the formation (Krapež and Martin, 1999; Pirajno et al., 2004).

### A.3. 2.45 Ga Brockman Iron Formation, Dales Gorge Member, Australia

The Brockman Iron Formation is a part of the Hamersley Supergroup located in the northwestern part of Australia (Cheney, 1996). The precursor sediments to BIF are interpreted to have been hydrothermal muds that were deposited on the flanks of submarine volcanoes and resedimented by density currents (Krapež et al., 2003). The age of the Brockman Iron Formation is well-constrained by U–Pb ages of zircons from ash beds within the iron formation (Pickard, 2002).

### A.4. 2.48 Ga Kuruman Iron Formation, South Africa

The Kuruman Iron Formation in South Africa was deposited on the Kaapvaal craton in the Griqualand West basin (Beukes and Gutzmer, 2008). In Supplementary information tables samples from the Kuruman are listed as being from the Koegas, Westerberg, and Kuruman area iron formations. Age constraints for the Kuruman Iron Formation come from U–Pb ages of zircons from tuffaceous sediments (Pickard, 2003).

### A.5. 2.5 Ga Benchmark Iron Formation, USA

The Benchmark Iron Formation is preserved in the Nemo area of the Black Hills uplift which is the easternmost Laramide exposure of the Archean Wyoming Province in the central United States (Bekker and Eriksson, 2003). The age constraints for the unit are based on U–Pb zircon geochronology of the Blue Draw Metagabbro (McCombs et al., 2004) that intrudes the early Paleoproterozoic rift sequence including the oxide-facies Benchmark Iron Formation (Bekker and Eriksson, 2003). The REE systematics of the Benchmark Iron Formation was discussed in Frei et al. (2008).

### A.6. 2.6 Ga Bjornevanns Iron Formation, Norway

The Bjornevanns Iron Formation is a part of the Fisketind Formation of the upper part of the Bjørnevann Group near Kirkenes in northern Norway and associated with amphibolites, locally containing pillow structures, hornblende gneisses, and subordinate quartz-biotite gneisses (Siedlecka et al., 1985). The iron formation is interpreted as a volcanic-exhalative deposit. The Bjørnevatn deposit sampled for our study represents the largest accumulation of BIF ores of this unit. The BIF ores consist of alternating magnetite- and quartz-dominated bands, 2–10 mm thick. Additional minerals in the ore include hornblende, grünerite, epidote, biotite, and hematite together with traces of pyrite and chalcopyrite that are mainly confined to the magnetite bands (Siedlecka et al., 1985). In some areas the BIF contain nearly monomineralic silicate facies bands of hornblende and grünerite. The ores were affected by three phases of isoclinal to tight folding and are crosscut by late orogenic granitic dykes and Mesoproterozoic dolerite dykes. The age is poorly constrained and based on U–Pb ages of a late orogenic granitic dyke cutting the Bjørnevann Group and a deformed pegmatite intruding the correlative Garsjø Complex. REE analysis of this iron formation was earlier reported by Derry and Jacobsen (1990).

### A.7. 2.7 Ga Manjeri Iron Formation, Zimbabwe

The Manjeri Formation is part of the volcano-sedimentary succession of the Belingwe Greenstone Belt and over-

lies older Neoarchean greenstone assemblage and basement gneisses. The Manjeri Formation is up to 250 m thick and contains conglomerates, shallow-water sandstones and stromatolitic limestones grading stratigraphically upwards into shale, graywacke, and iron formation. The iron formation does not appear to be directly linked to volcanic activity associated with the overlying komatiite-basalt sequence, although it is difficult to establish due to unresolved structural complexities. The age of the Manjeri Formation is poorly constrained and may be diachronous along strike. It is younger than an underlying $2831 \pm 6$ Ma greenstone succession, but older than or in part contemporaneous with a structurally overlying, ca. 2.7 Ga ultramafic to mafic subaqueous lava plain sequence (Hunter et al., 1998; Hofmann and Kusky, 2004). The Manjeri Formations has been correlated with similar successions in other greenstone belts of Zimbabwe (Prendergast, 2004). One of our samples (Z04-12) is derived from such unit from the Cactus Mine area of the Midlands greenstone belt.

### A.8. 2.72 Ga Mary River Iron Formation, Canada

Supracrustal rocks of the Mary River Group are located on northern Baffin Island, Canada. The samples are from the Mary River area. The iron formation is associated with mafic and ultramafic volcanics. Age constraints for the iron formation come from U–Pb zircon ages on associated felsic volcanics (Bethune and Scammell, 2003).

### A.9. 2.72 Ga Soudan Iron Formation, USA

The Soudan Iron Formation belongs to the Soudan Iron Formation Member of the Ely Greenstone in the Soudan Belt of the Vermillion District located in the northeastern part of Minnesota, United States. The iron formations are found in a volcanic-dominated sequence and their epiclastic equivalents. The iron formation is thought to be directly associated with seamount-type volcanic activity (Bayley and James, 1973). It is an oxide-facies cherty iron formation with hematite layers. The age of the Soudan iron formation is $2722 \pm 0.9$ Ma based on a U–Pb single zircon age of rhyolite from the Ely Greenstone (Peterson et al., 2001).

### A.10. 2.74 Ga Temagami Iron Formation, Canada

The Temagami Iron Formation is located in the Temagami Greenstone Belt in northern Ontario, Canada.

The iron formation occurs at or near the stratigraphic top of a metavolcanic sequence that is overlain by turbiditic metasedimentary rocks. Age constraints come from U–Pb zircon ages on a rhyolite flow underlying the iron formation and a rhyolite porphyry dike cutting andesitic flows above the iron formation (Bowins and Heaman, 1991).

### A.11. 2.9 Ga Steep Rock carbonate platform, ON, Canada

The Steep Rock Group of northwestern Ontario is situated in the Wabigoon Subprovince of the Superior Province. The 500 m thick Mosher carbonate was deposited in a diverse range of environments ranging from sabkha to subtidal as indicated by small domal stromatolites and microbial laminites grading upsection into large elongated stromatolite mounds potentially indicating upward-deepening (Kusky and Hudleston, 1999; Fralick et al., 2008). The age of this carbonate succession is poorly constrained between 3.0 and 2.7 Ga based on U–Pb dating in the Steep Rock Greenstone Belt (Tomlinson et al., 2003) but inferred to be close to 2.9 Ga based on regional correlations (Fralick et al., 2008). However, recent work suggest that the succession may be close to younger age constraint, ca. 2.7 Ga (Stone, 2010).

### A.12. 2.95 Ga Pongola Supergroup Iron Formation, South Africa

The Pongola Supergroup is located in eastern South Africa and southwestern Swaziland. The iron formation sampled for this study belongs to the Sinqeni Formation of the Mozaan Group (Beukes and Cairncross, 1991). The Mozaan Group sediments are thought to have been deposited on a broad marine shelf during thermal subsidence of the Pongola Basin. The Sinqeni Formation consists of quartz arenite, shale, and minor conglomerate and iron formation (Beukes and Cairncross, 1991). The 3–5 m thick iron formation occurs within shales of the Ijzermijn Member and was deposited on a shallow starved outer continental shelf during a time of maximum transgression (Beukes and Cairncross, 1991). The age for the Mozaan Group is based on U–Pb zircon dates for rhyolites within the Nsuze Group, which underlies the Mozaan Group (Hegner et al., 1994) and a pre-folding quartz porphyry sill that intruded the Mozaan Group (Gutzmer et al., 1999). REE systematics of the Sinqeni Iron Formation was recently studied in detail by Alexander et al. (2008).

### A.13. 2.95 Ga Witwatersrand Supergroup Iron Formation, South Africa

Iron formation of the Witwatersrand Supergroup sampled for this study belongs to the Contorted Bed of the Parktown Formation, West Rand Group. The iron formation has a sharp basal contact and a gradational upper contact and is up to 13 m thick. It sits within a shale and shale-siltstone succession and represents the condensed section at the base of an upward-coarsening cycle (Frimmel, 1996). The iron formation is composed of a magnetite-rich lower part with hematite and jasper at the very base and a siderite-rich upper part. The iron formation was likely deposited on a passive continental margin (Catuneanu, 2001). The age of the Witwatersrand Supergroup is reasonably well-constrained by U–Pb ages of overlying and underlying units, detrital zircons, and detrital and authigenic xenotimes (Armstrong et al., 1991; Kositcin and Krapež, 2004).

## APPENDIX B. SUPPLEMENTARY DATA

Supplementary data associated with this article can be found, in the online version, at doi:10.1016/j.gca.2010.07.021.

## REFERENCES


Ahn J. H. and Buseck P. R. (1990) Hematite nanospheres of possible colloidal origin from a Precambrian banded Fe formation. *Nature* **250**, 111–113.

Alexander B. W., Bau M., Andersson P. and Dulski P. (2008) Continentally-derived solutes in shallow Archean seawater: rare earth element and Nd isotope evidence in Fe formation from the 2.9 Ga Pongola Supergroup, South Africa. *Geochim. Cosmochim. Acta* **72**, 378–394.

Anbar A. D. and Holland H. D. (1992) The photochemistry of manganese and the origin of banded Fe formations. *Geochim. Cosmochim. Acta* **56**, 2595–2603.

Armstrong R. A., Compston W., Retief E. A., William L. S. and Welke H. J. (1991) Zircon ion microprobe studies bearing on the age and evolution of the Witwatersrand triad. *Precambrian Res.* **53**, 243–266.

Barley M. E., Pickard A. L. and Sylvester P. J. (1997) Emplacement of a large igneous province as a possible cause of banded Fe formation 2.45 billion years ago. *Nature* **385**, 55–58.

Bau M. (1993) Effects of syn-depositional and postdepositional processes on the rare-earth element distribution in Precambrian Iron-Formations. *Eur. J. Mineral.* **5**, 257–267.

Bau M. (1999) Scavenging of dissolved yttrium and rare earths by precipitating Fe oxyhydroxide: experimental evidence for Ce oxidation, Y–Ho fractionation, and lanthanide tetrad effect. *Geochim. Cosmochim. Acta* **63**, 67–77.

Bau M. and Alexander B. (2006) Preservation of primary REE patterns without Ce anomaly during dolomitization of Mid-Paleoproterozoic limestone and the potential re-establishment of marine anoxia immediately after the "Great Oxidation Event". *S. Afr. J. Geol.* **109**, 81–86.

Bau M. and Dulski P. (1996) Distribution of yttrium and rare-earth elements in the Penge and Kuruman Iron-Formations, Transvaal Supergroup, South Africa. *Precambrian Res.* **79**, 37–55.

Bau M. and Moller P. (1993) Rare-earth element systematics of the chemically precipitated component in early Precambrian Fe Formations and the evolution of the terrestrial atmosphere–hydrosphere–lithosphere system. *Geochim. Cosmochim. Acta* **57**, 2239–2249.

Bau M., Hohndorf A., Dulski P. and Beukes N. J. (1997a) Sources of rare-earth elements and Fe in paleoproterozoic iron-formations from the Transvaal Supergroup, South Africa: evidence from neodymium isotopes. *J. Geol.* **105**, 121–129.

Bau M., Moller P. and Dulski P. (1997b) Yttrium and lanthanides in eastern Mediterranean seawater and their fractionation during redox-cycling. *Mar. Chem.* **56**, 123–131.

Bayley R. W. and James H. L. (1973) Precambrian Iron-Formations of United-States. *Econ. Geol.* **68**, 934–959.

Bekker A. and Eriksson K. A. (2003) A Paleoproterozoic drowned carbonate platform on the southeastern margin of the Wyoming Craton: a record of the Kenorland breakup. *Precambrian Res.* **120**, 327–364.

Bekker A., Holland H. D., Wang P. L., Rumble D., Stein H. J., Hannah J. L., Coetzee L. L. and Beukes N. J. (2004) Dating the rise of atmospheric oxygen. *Nature* **427**, 117–120.

Bekker A., Slack J., Planavsky N., Krapež B., Hofmann A., Konhauser K. O. and Rouxel O. J. (2010) Iron formation: The sedimentary product of a complex interplay among mantle, tectonic, oceanic, and biospheric processes. *Econ. Geol.* **105**, 467–508.

Bethune K. M. and Scammell R. J. (2003) Geology, geochronology, and geochemistry of Archean rocks in the Eqe Bay area, north-central Baffin Island, Canada: constraints on the depositional and tectonic history of the Mary River Group of northeastern Rae Province. *Can. J. Earth Sci.* **40**, 1137–1167.

Beukes N. J. and Cairncross B. (1991) A lithostratigraphic-sedimentological reference profile for the Late Archean Mozaan Group, Pongola Sequence. application to sequence stratigraphy and correlation with the Witwatersrand Supergroup. *S. Afr. J. Geol.* **94**, 44–49.

Beukes N. J. and Gutzmer J. (2008) Origin and paleoenvironmental significance of major Fe Formations at the Archean–Paleoproterozoic boundary. *Soc. Econ. Geol. Rev.* **15**, 5–47.

Bowins R. J. and Heaman L. M. (1991) Age and timing of igneous activity in the Temagami greenstone belt, Ontario: a preliminary report. *Can. J. Earth Sci.* **28**, 1873–1876.

Braterman P. S., Cairnssmith A. G. and Sloper R. W. (1983) Photooxidation of hydrated Fe-2+—significance for banded Fe formations. *Nature* **303**, 163–164.

Byrne R. and Sholkovitz E. (1996) Marine chemistry and geochemistry of the lanthanides. In *Handbook on the Physics and Chemistry of the Rare Earths* (eds. K. A. Gschneider Jr. and L. Eyring). Elsevier, Amsterdam.

Canfield D. E. and Teske A. (1996) Late Proterozoic rise in atmospheric oxygen concentration inferred from phylogenetic and sulphur-isotope studies. *Nature* **382**, 127–132.

Catuneanu O. (2001) Flexural partitioning of the Late Archaean Witwatersrand foreland system, South Africa. *Sed. Geol.* **141**, 95–112.

Cheney E. S. (1996) Sequence stratigraphy and plate tectonic significance of the Transvaal succession of southern Africa and its equivalent in Western Australia. *Precambrian Res.* **79**, 3–24.

Clement B. G., Luther G. W. and Tebo B. M. (2009) Rapid, oxygen-dependent microbial Mn(II) oxidation kinetics at sub-micromolar oxygen concentrations in the Black Sea suboxic zone. *Geochim. Cosmochim. Acta* **73**, 1878–1889.

Cloud P. E. (1965) Significance of Gunflint (Precambrian) microflora—photosynthetic oxygen may have had important local effects before becoming a major atmospheric gas. *Science* **148**, 27–35.

Cloud P. (1973) Paleoecological significance of banded Iron-Formation. *Econ. Geol.* **68**, 1135–1143.

Crowe S. A., Jones C., Katsev S., Magen C., O'Neill A. H., Sturm A., Canfield D. E., Haffner G. D., Mucci A., Sundby B. and Fowle D. A. (2008) Photoferrotrophs thrive in an Archean Ocean analogue. *Proc. Natl. Acad. Sci.* **105**, 15938–15943.

de Baar H. J. W., German C. R., Elderfield H. and Vangaans P. (1988) Rare-earth element distributions in anoxic waters of the Cariaco Trench. *Geochim. Cosmochim. Acta* **52**, 1203–1219.

De Carlo E. H., Wen X.-Y. and Irving M. (2000) The influence of redox reactions on the uptake of dissolved Ce by suspended Fe and Mn oxide particles. *Aqua. Geochem.* **3**, 357–389.

De Carlo E. H. and Green W. J. (2002) Rare earth elements in the water column of Lake Vanda, McMurdo Dry Valleys, Antarctica. *Geochim. Cosmochim. Acta* **66**, 1323–1333.

Derry L. A. and Jacobsen S. B. (1988) The Nd and Sr isotopic evolution of proterozoic seawater. *Geophys. Res. Lett.* **15**, 397–400.

Derry L. A. and Jacobsen S. B. (1990) The chemical evolution of Precambrian seawater—evidence from REEs in banded Fe Formations. *Geochim. Cosmochim. Acta* **54**, 2965–2977.

Døssing L. N., Frei R., Stendal H. and Mapeo R. (2009) Characterization of enriched lithospheric mantle components in 2.7 Ga banded Fe formations: an example from the Tati Greenstone Belt, Northeastern Botswana. *Precambrian Res.* **172**, 334–356.

Edmonds H. N. and German C. R. (2004) Particle geochemistry in the Rainbow hydrothermal plume, Mid-Atlantic Ridge. *Geochim. Cosmochim. Acta* **68**, 759–772.

Edwards K. J., Rogers D. R., Wirsen C. O. and McCollom T. M. (2003) Isolation and characterization of novel psychrophilic,

neutrophilic, Fe-oxidizing, chemolithoautotrophic alpha- and, gamma-Proteobacteria from the deep sea. *Appl. Environ. Microbiol.* **69**, 2906–2913.

Eggins S. M., Woodhead J. D., Kinsley L. P. J., Mortimer G. E., Sylvester P., McCulloch M. T., Hergt J. M. and Handler M. R. (1997) A simple method for the precise determination of 40 trace elements in geological samples by ICPMS using enriched isotope internal standardization. *Chem. Geol.* **134**, 311–326.

Fischer W. W., Schroeder S., Lacassie J. P., Beukes N. J., Goldberg T., Strauss H., Horstmann U. E., Schrag D. P. and Knoll A. H. (2009) Isotopic constraints on the Late Archean carbon cycle from the Transvaal Supergroup along the western margin of the Kaapvaal Craton, South Africa. *Precambrian Res.* **169**, 15–27.

Foustoukos D. I. and Bekker A. (2008) Hydrothermal Fe(II) oxidation during phase separation: relevance to the origin of Algoma-type BIFs. *Geochim. Cosmochim. Acta* **72**, A280.

Fralick P., Davis D. W. and Kissin S. A. (2002) The age of the Gunflint Formation, Ontario, Canada: single zircon U-Pb age determinations from reworked volcanic ash. *Can. J. Earth Sci.* **39**, 1085–1091.

Fralick P., Hollings P. and King P. (2008) Stratigraphy, geochemistry, and depositional environments of Mesoarchean sedimentary units in western Superior Province. Implications for generation of early crust. *Geol. Soc. Am. Special Pap.* **440**, 77–96.

Frei R., Dahl P. S., Duke E. F., Frei K. M., Hansen T. R., Frandsson M. M. and Jensen L. A. (2008) Trace element and isotopic characterization of Neoarchean and Paleoproterozoic Fe formations in the Black Hills (South Dakota, USA): assessment of chemical change during 2.9–1.9 Ga deposition bracketing the 2.4–2.2 Ga first rise of atmospheric oxygen. *Precambrian Res.* **162**, 441–474.

Frimmel H. E. (1996) Witwatersrand iron-formations and their significance for gold genesis and the composition limits of orthoamphibole. *Mineral. Petrol.* **56**, 273–295.

Fryer B. J. (1976) Rare earth evidence in iron-formations for changing Precambrian oxidation states. *Geochim. Cosmochim. Acta* **41**, 361–367.

Garrels R. M. and Perry E. A. J. (1974) Cycling of carbon, sulfur, and oxygen through geologic time. In *The Sea* (ed. E. A. Goldberg). Wiley, New York.

German C. R. and Elderfield H. (1990) Application of the Ce-anomaly as a paleoredox indicator: the ground rules. *Paleoceanography* **5**, 823–833.

German C. R., Holliday B. P. and Elderfield H. (1991) Redox cycling of rare earth elements in the suboxic zone of the Black Sea. *Geochim. Cosmochim. Acta* **55**, 3553–3558.

Gutzmer J., Nhleko N., Beukes N. J., Pickard A. and Barley M. E. (1999) Geochemistry and ion microprobe (SHRIMP) age of a quartz porphyry sill in the Mozaan Group of the Pongola Supergroup: implications for the Pongola and Witwatersrand supergroups. *S. Afr. J. Geol.* **102**, 139–146.

Habicht K. S., Gade M., Thamdrup B., Berg P. and Canfield D. E. (2002) Calibration of sulfate levels in the Archean Ocean. *Science* **298**, 2372–2374.

Haley B. A., Klinkhammer G. P. and McManus J. (2004) Rare earth elements in pore waters of marine sediments. *Geochim. Cosmochim. Acta* **68**, 1265–1279.

Harder E. C. (1919) Iron-depositing bacteria and their geological relations. USGS Professional Paper, **113**, 89p.

Hegner E., Kröner A. and Hunt P. (1994) A precise U–Pb zircon age for the Archaean Pongola Supergroup volcanics in Swaziland. *J. Afr. Earth Sci.* **18**, 339–341.

Hofmann A. and Kusky T. M. (2004) The Belingwe greenstone belt: ensialic or oceanic? In *Precambrian Ophiolites and Related Rocks. Developments in Precambrian Geology*, vol. 13 (ed. T. M. Kusky). Elsevier, Amsterdam, pp. 487–537.

Holland H. D. (1973) Oceans—possible source of Fe in Iron-Formations. *Econ. Geol.* **68**, 1169–1172.

Holland H. D. (1984) *The Chemical Evolution of the Atmosphere and Oceans*. Princeton University Press, Princeton, NJ.

Holland H. D. (2005) 100th anniversary special paper: sedimentary mineral deposits and the evolution of earth's near-surface environments. *Econ. Geol.* **100**, 1489–1509.

Hunter M. A., Bickle M. J., Nisbet E. G., Martin A. and Chapman H. J. (1998) Continental extensional setting for the Archean Belingwe Greenstone Belt, Zimbabwe. *Geology* **26**, 883–886.

Isley A. E. and Abbott D. H. (1999) Plume-related mafic volcanism and the deposition of banded Fe formation. *J. Geophys. Res. (Solid Earth)* **104**, 15461–15477.

Johnson C. M., Beard B. L., Roden E. E., Newman D. K. and Nealson K. H. (2004) Isotopic constraints on biogeochemical cycling of Fe. *Geochem. Nontradit. Stable Isot.* **55**, 359–408.

Johnson C. M., Beard B. L., Klein C., Beukes N. J. and Roden E. E. (2008) Fe isotopes constrain biologic and abiologic processes in banded Fe formation genesis. *Geochim. Cosmochim. Acta* **72**, 151–169.

Kamber B. S. (2009) Geochemical fingerprinting: 40 years of analytical development and real world applications. *Appl. Geochem.* **24**, 1074–1086.

Kamber B. S. and Webb G. E. (2001) The geochemistry of late Archaean microbial carbonate: implications for ocean chemistry and continental erosion history. *Geochim. Cosmochim. Acta* **65**, 2509–2525.

Kappler A., Pasquero C., Konhauser K. O. and Newman D. K. (2005) Deposition of banded Fe formations by anoxygenic phototrophic Fe(II)-oxidizing bacteria. *Geology* **33**, 865–868.

Kato Y., Kawakami T., Kano T., Kunugiza K. and Swamy N. S. (1996) Rare-earth element geochemistry of banded Fe formations and associated amphibolite from the Sargur belts, south India. *J. SE Asian Earth Sci.* **14**, 161–164.

Kato Y., Ohta I., Tsunematsu T., Watanabe Y., Isozaki Y., Maruyama S. and Imai N. (1998) Rare earth element variations in mid-Archean banded Fe formations: implications for the chemistry of ocean and continent and plate tectonics. *Geochim. Cosmochim. Acta* **62**, 3475–3497.

Kato Y., Kano T. and Kunugiza K. (2002) Negative Ce anomaly in the Indian banded Fe formations: evidence for the emergence of oxygenated deep-sea at 2.9 similar to 2.7 Ga. *Resour. Geol.* **52**, 101–110.

Kato Y., Yamaguchi K. E. and Ohmoto H. (2006) Rare earth elements in Precambrian banded Fe formations: secular changes of Ce and Eu anomalies and evolution of atmospheric oxygen. In *Evolution of the Atmosphere, Hydrosphere, and Biosphere on Early Earth: Constraints from Ore Deposits* (eds. S. E. Kessler and H. Ohmoto). Geological Society of America, Denver.

Kaufman A. J., Hayes J. M. and Klein C. (1990) Primary and diagenetic controls of isotopic compositions of Iron-Formation carbonates. *Geochim. Cosmochim. Acta* **54**, 3461–3473.

Khan R. M. K. and Naqvi S. M. (1996) Geology, geochemistry and genesis of BIF of Kushtagi schist belt, Archaean Dharwar Craton, India. *Miner. Deposita* **31**, 123–133.

Klein C. (2005) Some Precambrian banded iron-formations (BIFs) from around the world: their age, geologic setting, mineralogy, metamorphism, geochemistry, and origin. *Am. Mineral.* **90**, 1473–1499.

Klein C. and Beukes N. J. (1989) Geochemistry and sedimentology of a facies transition from limestone to Iron-Formation Deposition in the Early Proterozoic Transvaal Supergroup, South-Africa. *Econ. Geol.* **84**, 1733–1774.

Klinkhammer G., Elderfield H. and Hudson A. (1983) Rare-Earth elements in seawater near hydrothermal vents. *Nature* **305**, 185–188.

Koeppenkastrop D. and De Carlo E. H. (1992) Sorption of rare-Earth elements from seawater onto synthetic mineral particles—an experimental approach. *Chem. Geol.* **95**, 251–263.

Konhauser K. O., Hamade T., Raiswell R., Morris R. C., Ferris F. G., Southam G. and Canfield D. E. (2002) Could bacteria have formed the Precambrian banded Fe formations? *Geology* **30**, 1079–1082.

Konhauser K. O., Amskold L., Lalonde S. V., Posth N. R., Kappler A. and Anbar A. (2007) Decoupling photochemical Fe(II) oxidation from shallow-water BIF deposition. *Earth Planet. Sci. Lett.* **258**, 87–100.

Kositcin N. and Krapež B. (2004) SHRIMP U–Pb detrital zircon geochronology of the Late Archaean Witwatersrand Basin of South Africa: relation between zircon provenance age spectra and basin evolution. *Precambrian Res.* **129**, 141–168.

Krapež B. and Martin D. (1999) Sequence stratigraphy of the Palaeoproterozoic Nabberu Province of Western Australia. *Aust. J. Earth Sci.* **46**, 89–103.

Krapež B., Barley M. E. and Pickard A. L. (2003) Hydrothermal and resedimented origins of the precursor sediments to banded iron formation: sedimentological evidence from the Early Palaeoproterozoic Brockman Supersequence of Western Australia. *Sedimentology* **50**, 979–1011.

Kump L. R. and Seyfried W. E. (2005) Hydrothermal Fe fluxes during the Precambrian: effect of low oceanic sulfate concentrations and low hydrostatic pressure on the composition of black smokers. *Earth Planet. Sci. Lett.* **235**, 654–662.

Kusky T. P. and Hudleston P. J. (1999) Growth and demise of an Archean carbonate platform, Steep Rock Lake, Ontario, Canada. *Can. J. Earth Sci.* **36**, 565–584.

McCombs J. A., Dahl P. S. and Hamilton M. A. (2004) U–Pb ages of Neoarchean granitoids from the Black Hills, South Dakota, USA: implications for crustal evolution in the Archean Wyoming province. *Precambrian Res.* **130**, 161–184.

Moffett J. W. (1994) The relationship between cerium and manganese oxidation in the marine-environment. *Limnol. Oceanogr.* **39**, 1309–1318.

Moller P. and Bau M. (1993) Rare-Earth patterns with positive cerium anomaly in alkaline waters from Lake Van, Turkey. *Earth Planet. Sci. Lett.* **117**, 671–676.

Nothdurft L. D., Webb G. E. and Kamber B. S. (2004) Rare earth element geochemistry of Late Devonian reefal carbonates, canning basin, Western Australia: confirmation of a seawater REE proxy in ancient limestones. *Geochim. Cosmochim. Acta* **68**, 263–283.

Nozaki Y., Zhang J. and Amakawa H. (1997) The fractionation between Y and Ho in the marine environment. *Earth Planet. Sci. Lett.* **148**, 329–340.

Ohmoto H., Watanabe Y. and Kumazawa K. (2004) Evidence from massive siderite beds for a $CO_2$-rich atmosphere before, 1.8 billion years ago. *Nature* **429**, 395–399.

Ohmoto H., Watanabe Y., Yamaguchi K. E., Naraoka H., Kakegawa T., Haruna M., Hayashi K. and Kato Y. (2006) Chemical and biological evolution of early Earth: constraints from banded iron-formations. In *Evolution of the Atmosphere, Hydrosphere, and Biosphere on Early Earth: Constraints from Ore Deposits* (eds. S. E. Kessler and H. Ohmoto). Geological Society of America, Denver.

Ohta A. and Kawabe I. (2001) REE(III) adsorption onto Mn dioxide (δ-$MnO_2$) and Fe oxyhydroxide: Ce(III) oxidation by δ-$MnO_2$. *Geochim. Cosmochim.* **65**, 695–703.

Ojakangas R. W., Morey G. B. and Southwick D. L. (2001) Paleoproterozoic basin development and sedimentation in the Lake Superior region, North America. *Sed. Geol.* **141**, 319–341.

Pecoits E., Gingras M. K., Barley M. E., Kappler A., Posth N. R. and Konhauser K. O. (2009) Petrography and geochemistry of the Dales Gorge banded Fe formation: paragenetic sequence, source and implications for palaeo-ocean chemistry. *Precambrian Res.* **172**, 163–187.

Peterson D. M., Gallup C., Jirsa M. A. and Davis D. W. (2001) Correlation of Archean assemblages across the U.S.–Canadian border: phase I geochronology. *Proc. Inst. Lake Super. Geol.* **47**, 77–78.

Pickard A. L. (2002) SHRIMP U–Pb zircon ages of tuffaceous mudrocks in the Brockman Fe Formation of the Hamersley Range, Western Australia. *Aust. J. Earth Sci.* **49**, 491–507.

Pickard A. L. (2003) SHRIMP U–Pb zircon ages for the Palaeoproterozoic Kuruman Fe Formation, Northern Cape Province, South Africa: evidence for simultaneous BIF deposition on Kaapvaal and Pilbara Cratons. *Precambrian Res.* **125**, 275–315.

Pirajno F., Jones J. A., Hocking R. M. and Halilovic J. (2004) Geology and tectonic evolution of Palaeoproterozoic basins of the eastern Capricorn Orogen, Western Australia. *Precambrian Res.* **128**, 315–342.

Planavsky N., Rouxel O., Bekker A., Shapiro R., Fralick P. and Knudsen A. (2009) Iron-oxidizing microbial ecosystems thrived in late Paleoproterozoic redox-stratified oceans. *Earth Planet. Sci. Lett.* **286**, 230–242.

Poulton S. W., Fralick P. W. and Canfield D. E. (2004) The transition to a sulphidic ocean similar to 1.84 billion years ago. *Nature* **431**, 173–177.

Prakash H. S. M. and Devapriyan G. V. (1996) REE enrichment in the oxide facies BIF of Chitradurga schist belt, Karnataka. *J. Geol. Soc. India* **47**, 265.

Prendergast M. D. (2004) The Bulawayan Supergroup: a late Archaean passive margin-related large igneous province in the Zimbabwe craton. *J. Geol. Soc.* **161**, 431–445.

Quinn K. A., Byrne R. H. and Schijf J. (2006) Sorption of yttrium and rare earth elements by amorphous ferric hydroxide: influence of solution complexation with carbonate. *Geochim. Cosmochim. Acta* **70**, 4151–4165.

Schijf J., de Baar H. J. W. and Millero F. J. (1995) Vertical distributions and speciation of dissolved rare earth elements in the anoxic brines of Bannock Basin, eastern Mediterranean. *Geochim. Cosmochim. Acta* **57**, 1419–1432.

Schneider D. A., Bickford M. E., Cannon W. F., Schulz K. J. and Hamilton M. A. (2002) Age of volcanic rocks and syndepositional iron formations, Marquette Range Supergroup: implications for the tectonic setting of Paleoproterozoic, iron formations of the Lake Superior region. *Can. J. Earth Sci.* **39**, 999–1012.

Schulz K. J. and Cannon W. F. (2007) The penokean orogeny in the lake superior region. *Precambrian Res.* **157**, 4–25.

Sherrel R. M., Field M. P. and Ravizza G. (1999) Uptake and fractionation of rare earth elements on hydrothermal plume particles at 9 45′N, East Pacific Rise. *Geochim. Cosmochim. Acta* **63**, 1709–1722.

Sholkovitz E. R. and Elderfield H. (1988) Cycling of dissolved rare earth elements in Chesapeake Bay. *Global Biogeochem. Cycles* **2**, 157–176.

Sholkovitz E. R., Shaw T. and Schneider D. L. (1992) The geochemistry of rare earth elements in the seasonally anoxic water column and porewaters of Chesapeake Bay. *Geochim. Cosmochim. Acta* **56**, 3389–3402.

Sholkovitz E. R., Landing W. M. and Lewis B. L. (1994) Ocean particle chemistry: the fractionation of rare earth elements between suspended particles and seawater. *Geochim. Cosmochim. Acta* **58**, 1567–1580.

Siedlecka A., Iversen E., Krill A. G., Lieungh B., Often M., Sandstad J. S. and Solli A. (1985) Lithostratigraphy and correlation of the Archean and Early Proterozic rocks of

Finnmarksvidda and Sorvaranger district. *Nor. Geol. Unders.* **403**, 7–36.

Slack J. F., Grenne T., Bekker A., Rouxel O. J. and Lindberg P. A. (2007) Suboxic deep seawater in the late Paleoproterozoic: evidence from hematitic chert and Fe formation related to seafloor-hydrothermal sulfide deposits, central Arizona, USA. *Earth Planet. Sci. Lett.* **255**, 243–256.

Spier C. A., de Oliveira S. M. B., Sial A. N. and Rios F. J. (2007) Geochemistry and genesis of the banded Fe formations of the Caue Formation, Quadrilatero Ferrifero, Minas Gerais, Brazil. *Precambrian Res.* **152**, 170–206.

Stone D. (2010) Precambrian geology of the central Wabigoon Subprovince area, northwestern Ontario, Ontario Geological Survey, Open File Report 5422, 130p.

Sumner D. Y. (1997) Carbonate precipitation and oxygen stratification in late Archean seawater as deduced from facies and stratigraphy of the Gamohaan and Frisco formations, Transvaal Supergroup, South Africa. *Am. J. Sci.* **297**, 455–487.

Sumner D. Y. and Grotzinger J. P. (2004) Implications for Neoarchaean ocean chemistry from primary carbonate mineralogy of the Campbellrand-Malmani Platform, South Africa. *Sedimentology* **51**, 1273–1299.

Tomlinson K., Davis D., Stone D. and Hart T. (2003) U-Pb age and Nd isotopic evidence for Archean terrane development and crustal recycling in the south-central Wabigoon subprovince, Canada. *Contrib. Mineral. Petrol.* **144**, 684–702.

Veizer J., Hoefs J., Lowe D. R. and Thurston P. C. (1989) Geochemistry of Precambrian carbonates: II. Archean greenstone belts and Archean sea-water. *Geochim. Cosmochim. Acta* **53**, 859–871.

Walker J. C. G. (1984) Suboxic diagenesis in banded Fe formations. *Nature* **309**, 340–342.

Webb G. E. and Kamber B. S. (2000) Rare earth elements in Holocene reefal microbialites: A new shallow seawater proxy. *Geochim. Cosmochim. Acta* **64**, 1557–1565.

Widdel F., Schnell S., Heising S., Ehrenreich A., Assmus B. and Schink B. (1993) Ferrous Fe oxidation by anoxygenic phototrophic bacteria. *Nature* **362**, 834–836.

*Associate editor:* Robert H. Byrne